

# Status of Six-field Two-fluid Models in BOUT++



**Tianyang Xia<sup>1,2</sup>, X.Q. Xu<sup>2</sup> and BOUT++ team**

<sup>1</sup>Institute of Plasma Physics, Chinese Academy of Sciences, Hefei, China.

<sup>2</sup>Lawrence Livermore National Laboratory, Livermore, CA 94550, USA

**2015 BOUT++ mini workshop  
December 16th, 2013**





- Introduction of 6-field 2-fluid model
- Applications for divertor simulations
  - Transient heat flux simulations during ELM bursts on DIII-D
    - ◆ Kinetic modification on thermal conduction in pedestal
    - ◆ Validation with experiments
    - ◆ Study on the effects of magnetic flutter in parallel conduction
  - Transient particle flux simulations during ELM bursts on EAST
  - Summary for divertor simulations
- Demo for running 6-field



- Introduction of 6-field 2-fluid model
- Applications for divertor simulations
  - Transient heat flux simulations during ELM bursts on DIII-D
    - ◆ Kinetic modification on thermal conduction in pedestal
    - ◆ Validation with experiments
    - ◆ Study on the effects of magnetic flutter in parallel conduction
  - Transient particle flux simulations during ELM bursts on EAST
  - Summary for divertor simulations
- Demo for running 6-field



Six-field two-fluid model is necessary to describe:

- pedestal energy loss
- density profile evolution through the ELM event,
- heat flux
- energy depositions on divertor target
- Edge turbulence

Six-field ( $\varpi$ ,  $n_i$ ,  $T_i$ ,  $T_e$ ,  $A_{||}$ ,  $V_{||}$ ): based on Braginskii equations, the density, momentum and energy of ions and electrons are described in drift ordering[1,2].

---

[1]X. Q. Xu et al., *Commun. Comput. Phys.* **4**, 949 (2008).

[2]T. Y. Xia et al., *Nucl. Fusion* **53**, 073009 (2013).



# Equations of 6-field 2-fluid model



$$\frac{\partial}{\partial t} \varpi = -\frac{1}{B_0} \mathbf{b} \times \nabla_{\perp} \Phi \cdot \nabla \varpi + B_0^2 \nabla_{\parallel} \left( \frac{J_{\parallel}}{B_0} \right) + 2\mathbf{b} \times \boldsymbol{\kappa} \cdot \nabla p_i$$

$$- \frac{1}{2\Omega_i} \left[ \frac{1}{B_0} \mathbf{b} \times \nabla P_i \cdot \nabla (\nabla_{\perp}^2 \Phi) - Z_i e B_0 \mathbf{b} \times \nabla n_i \cdot \nabla \left( \frac{\nabla_{\perp} \Phi}{B_0} \right)^2 \right]$$

$$+ \frac{1}{2\Omega_i} \left[ \frac{1}{B_0} \mathbf{b} \times \nabla \Phi \cdot \nabla (\nabla_{\perp}^2 P_i) - \nabla_{\perp}^2 \left( \frac{1}{B_0} \mathbf{b} \times \nabla \Phi \cdot \nabla P_i \right) \right] + \mu_{\parallel i} \nabla_{\parallel 0}^2 \varpi, \quad (1)$$

$$\frac{\partial}{\partial t} n_i = -\frac{1}{B_0} \mathbf{b} \times \nabla_{\perp} \Phi \cdot \nabla n_i - \frac{2n_i}{B_0} \mathbf{b} \times \boldsymbol{\kappa} \cdot \nabla \Phi$$

$$- \frac{2}{Z_i e B_0} \mathbf{b} \times \boldsymbol{\kappa} \cdot \nabla P_i - n_i B_0 \nabla_{\parallel} \left( \frac{V_{\parallel i}}{B_0} \right), \quad (2)$$

$$\frac{\partial}{\partial t} V_{\parallel i} = -\frac{1}{B_0} \mathbf{b} \times \nabla_{\perp} \Phi \cdot \nabla V_{\parallel i} - \frac{1}{m_i n_{i0}} \mathbf{b} \cdot \nabla P, \quad (3)$$

$$\frac{\partial}{\partial t} A_{\parallel} = -\nabla_{\parallel} \phi + \frac{\eta}{\mu_0} \nabla_{\perp}^2 A_{\parallel} + \frac{1}{e n_{e0} B_0} \nabla_{\parallel} P_e + \frac{0.71 k_B}{e B_0} \nabla_{\parallel} T_e - \frac{\eta H}{\mu_0} \nabla_{\perp}^4 A_{\parallel}, \quad (4)$$

$$\frac{\partial}{\partial t} T_i = -\frac{1}{B_0} \mathbf{b} \times \nabla_{\perp} \Phi \cdot \nabla T_i$$

$$- \frac{2}{3} T_i \left[ \left( \frac{2}{B_0} \mathbf{b} \times \boldsymbol{\kappa} \right) \cdot \left( \nabla \Phi + \frac{1}{Z_i e n_{i0}} \nabla P_i + \frac{5}{2} \frac{k_B}{Z_i e} \nabla T_i \right) + B_0 \nabla_{\parallel} \left( \frac{V_{\parallel i}}{B_0} \right) \right]$$

$$+ \frac{2}{3 n_{i0} k_B} \nabla_{\parallel 0} (\kappa_{\parallel i} \nabla_{\parallel 0} T_i) + \frac{2}{3 n_{i0} k_B} \nabla_{\perp} \cdot (\kappa_{\perp i} \nabla_{\perp} T_i) + \frac{2 m_e Z_i}{m_i \tau_e} (T_e - T_i), \quad (5)$$

$$\frac{\partial}{\partial t} T_e = -\frac{1}{B_0} \mathbf{b} \times \nabla_{\perp} \Phi \cdot \nabla T_e$$

$$- \frac{2}{3} T_e \left[ \left( \frac{2}{B_0} \mathbf{b} \times \boldsymbol{\kappa} \right) \cdot \left( \nabla \Phi - \frac{1}{e n_{e0}} \nabla P_e - \frac{5}{2} \frac{k_B}{e} \nabla T_e \right) + B_0 \nabla_{\parallel} \left( \frac{V_{\parallel e}}{B_0} \right) \right]$$

$$+ 0.71 \frac{2 T_e}{3 e n_{e0}} B_0 \nabla_{\parallel} \left( \frac{J_{\parallel}}{B_0} \right) + \frac{2}{3 n_{e0} k_B} \nabla_{\parallel 0} (\kappa_{\parallel e} \nabla_{\parallel 0} T_e) + \frac{2}{3 n_{e0} k_B} \nabla_{\perp} \cdot (\kappa_{\perp e} \nabla_{\perp} T_e)$$

$$- \frac{2 m_e}{m_i} \frac{1}{\tau_e} (T_e - T_i) + \frac{2}{3 n_{e0} k_B} \eta_{\parallel} J_{\parallel}^2, \quad (6)$$

Compressible terms
Parallel velocity terms
Electron Hall
Thermal force
Gyro-viscosity
Energy exchange
Energy flux
Thermal conduction



# The background impurity is taken into account in order to use full set of measured profiles



The vorticity equation with background impurity is modified to

$$\begin{aligned} \frac{\partial}{\partial t} \varpi &= - \left( \frac{1}{B_0} \mathbf{b} \times \nabla_{\perp} \Phi + V_{\parallel i} \mathbf{b} \right) \cdot \nabla \varpi + B^2 \nabla_{\parallel} \left( \frac{J_{\parallel}}{B} \right) + 2 \mathbf{b} \times \boldsymbol{\kappa} \cdot \nabla p_1 \\ &\quad - \frac{1}{2\Omega_i} \left[ \frac{1}{B} \mathbf{b} \times \nabla P_i \cdot \nabla (\nabla_{\perp}^2 \Phi) - Z_i e B \mathbf{b} \times \nabla n_i \cdot \nabla \left( \frac{\nabla_{\perp} \Phi}{B} \right)^2 \right] \\ &\quad + \frac{1}{2\Omega_i} \left[ \frac{1}{B} \mathbf{b} \times \nabla \Phi \cdot \nabla (\nabla_{\perp}^2 P_i) - \nabla_{\perp}^2 \left( \frac{1}{B} \mathbf{b} \times \nabla \Phi \cdot \nabla P_i \right) \right] \\ &\quad - \frac{1}{2\Omega_{im}} \left[ n_{im} Z_{im} e V_{Dim} \cdot \nabla (\nabla_{\perp}^2 \Phi) - m_{im} \Omega_{im} \mathbf{b} \times \nabla n_{im} \cdot \nabla V_E^2 \right] \\ &\quad + \frac{1}{2\Omega_{im}} \left[ \mathbf{V}_E \cdot \nabla (\nabla_{\perp}^2 P_{im}) - \nabla_{\perp}^2 (\mathbf{V}_E \cdot \nabla P_{im}) \right]. \end{aligned}$$

Gyro-viscous

$$\begin{aligned} \varpi &= \mathbf{b} \cdot \nabla \times (m_i n_i V_i + m_{im} n_{im} V_{im}) \\ &\simeq n_{i0} \frac{m_i}{B_0} \left( \nabla_{\perp}^2 \phi + \frac{1}{n_{i0}} \nabla_{\perp} \phi \cdot \nabla_{\perp} n_{i0} + \frac{1}{n_{i0} Z_i e} \nabla_{\perp}^2 p_{i1} \right) \\ &\quad + n_{im} \frac{m_{im}}{B_0} \left( \nabla_{\perp}^2 \phi + \frac{1}{n_{im}} \nabla_{\perp} \phi \cdot \nabla_{\perp} n_{im} \right). \end{aligned}$$

Quasi-neutral condition

$$Z_i n_{i0} + Z_{im} n_{im} = n_{e0}$$

$$n_j = n_{j0} + n_{j1},$$

$$P_j = P_{j0} + p_{j1},$$

$$P = P_i + P_e + P_{im} = P_0 + p_1 = (P_{i0} + P_{e0}) + (p_{i1} + p_{e1}) + P_{im},$$

$$\Phi = \Phi_0 + \phi,$$

$$J_{\parallel} = J_{\parallel 0} + J_{\parallel 1},$$

$$V_{\parallel e} = \frac{Z_i n_i}{n_e} V_{\parallel i} - \frac{J_{\parallel 1}}{en_e},$$

$$\mathbf{b} = \mathbf{b}_0 - \mathbf{b}_0 \times \nabla \psi,$$

$$J_{\parallel 1} = -\frac{1}{\mu_0} B_0 \nabla_{\perp}^2 \psi.$$

The effects of impurity: all the terms are at the order of  $m_{im} n_{im}$



# The physics switches of 6-field model in BOUT++



Switch Name	Physics meanings
compress0	Parallel velocity
continuity	Compressible terms
eHall	Electron Hall effects
energy_flux	Energy flux terms
energy_exch	Energy exchange terms
thermal_force	Thermal force terms
gyro_viscous	Gyro-viscosity
viscos_par	Parallel viscosity
spitzer_resist	Spitzer resistivity
hyperresist	Hyper resistivity
diffusion_par	Thermal conduction
experimental_Er	Using measured $E_r$
impurity_prof	Including the background impurity



# Boundary conditions and normalizations



Boundary conditions:

Inner boundary:

$$\partial n_i / \partial \Psi = 0, \quad \partial T_j / \partial \Psi = 0, \quad \varpi = 0, \quad \nabla_{\perp}^2 A_{\parallel} = 0, \quad \partial^2 \phi / \partial^2 \Psi = 0, \quad \partial V_{\parallel} / \partial \Psi = 0$$

Outer boundary:

$$n_i = 0, \quad T_j = 0, \quad \varpi = 0, \quad \nabla_{\perp}^2 A_{\parallel} = 0, \quad \partial^2 \phi / \partial^2 \Psi = 0, \quad V_{\parallel} = 0$$

Normalizations:

$$\begin{aligned} \hat{T}_j &= \frac{T_j}{\bar{T}_j}, & \hat{n} &= \frac{n_i}{\bar{n}}, & \hat{L} &= \frac{L}{\bar{L}}, \\ \hat{t} &= \frac{t}{\bar{t}}, & \hat{B} &= \frac{B}{\bar{B}}, & \hat{J} &= \frac{\mu_0 \bar{L}}{B_0} J, \\ \hat{\psi} &= \frac{\psi}{\bar{L}}, & \hat{\phi} &= \frac{\bar{t}}{L^2 B_0} \phi, & \hat{\varpi} &= \frac{\bar{t}}{m_i \bar{n}} \varpi, \\ \tau &= \frac{\bar{T}_i}{\bar{T}_e}, & \hat{V} &= \frac{V}{V_A}, & V_A &= \frac{\bar{L}}{\bar{t}} = \frac{\bar{B}}{\sqrt{\mu_0 m_i \bar{n}_i}}, \\ \hat{P}_j &= \frac{P_j}{k_B \bar{n} \bar{T}_j}, & \hat{\kappa} &= \bar{L} \kappa, & \hat{\nabla} &= \bar{L} \nabla \end{aligned}$$



# 3-field 2-fluid model is good enough to simulate P-B stability and ELM crashes, additional physics from multi-field contributes less than 25% corrections



## Fundamental physics in ELMs:

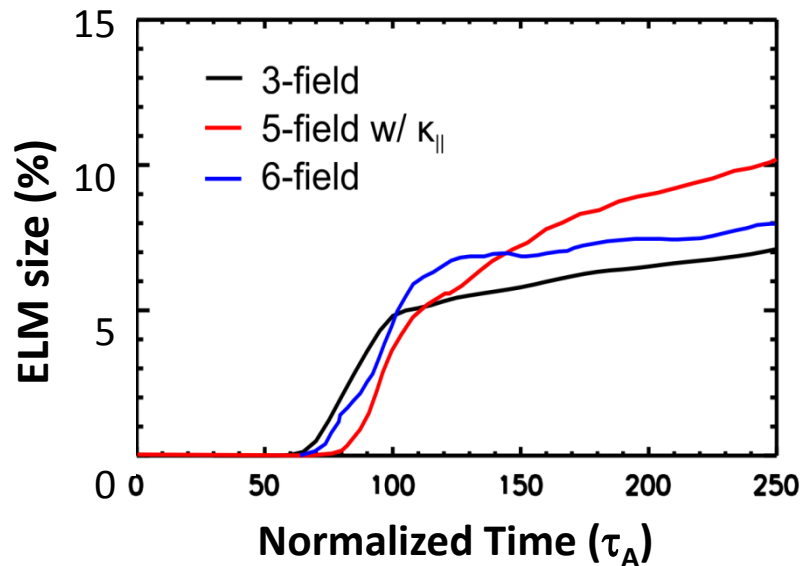
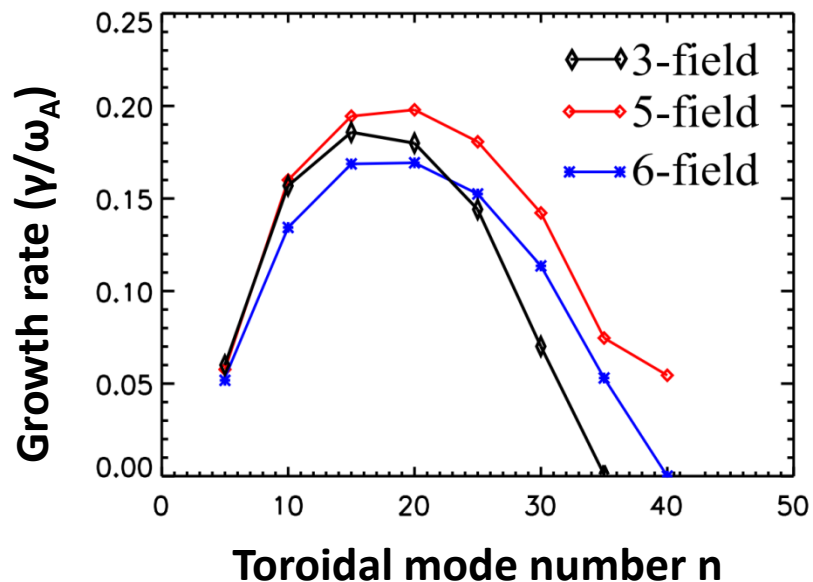
- ✓ Peeling-Ballooning instability
- ✓ Ion diamagnetic stabilization
  - kinetic effect
- ✓ Resistivity and hyper-resistivity
  - reconnection

## Additional physics:

- Ion acoustic waves
- Thermal conductivities
- Hall effect
- Compressibility
- Electron-ion friction

change the linear growth rate less than **25%**

Power depositions on PFCs.  
Turbulence and transport



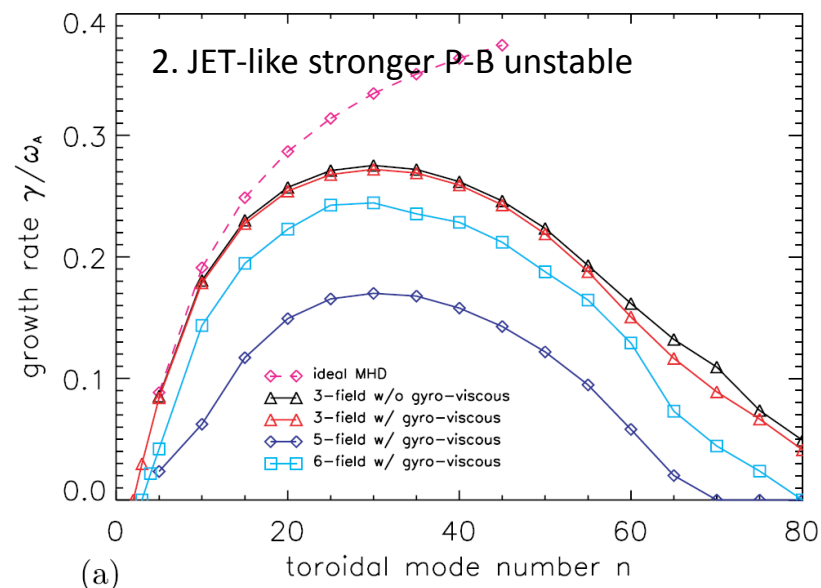
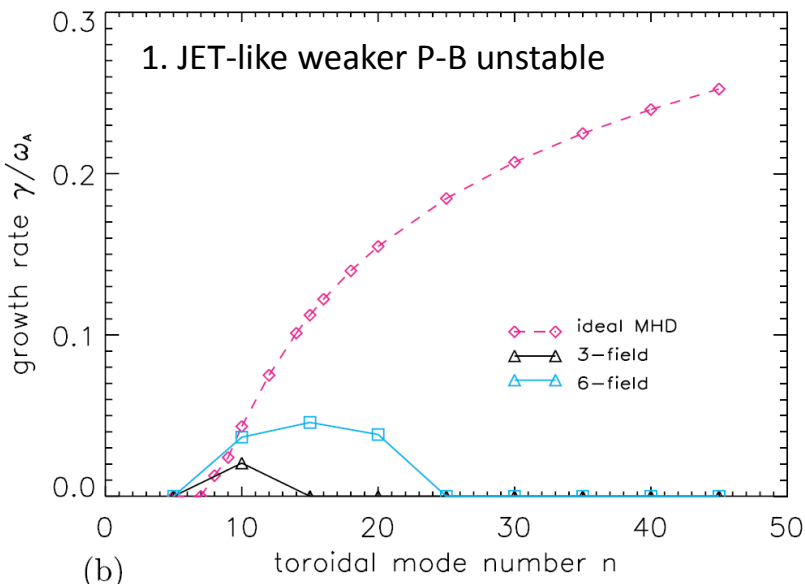
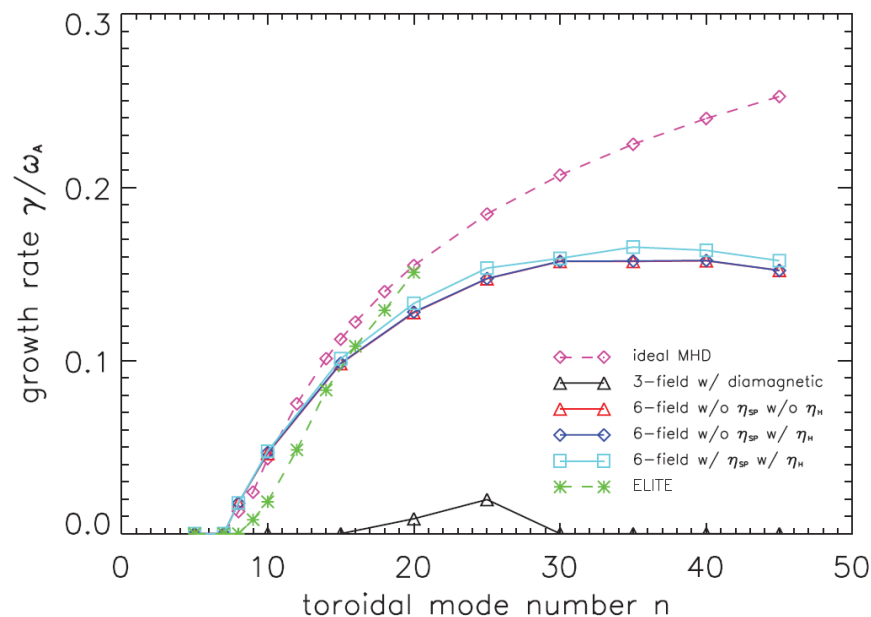


# Benchmark with ELITE and 3-field mode in BOUT++



For a typical peeling-ballooning mode unstable equilibrium:

- Ideal MHD, the growth rate is well consistent with ELITE.
- Full 6-field mode gives smaller growthrate than ideal MHD, mostly due to FLR effects.
- Higher than 3-field model w/ diamagnetic effects, most due to electromagnetic drift wave instability





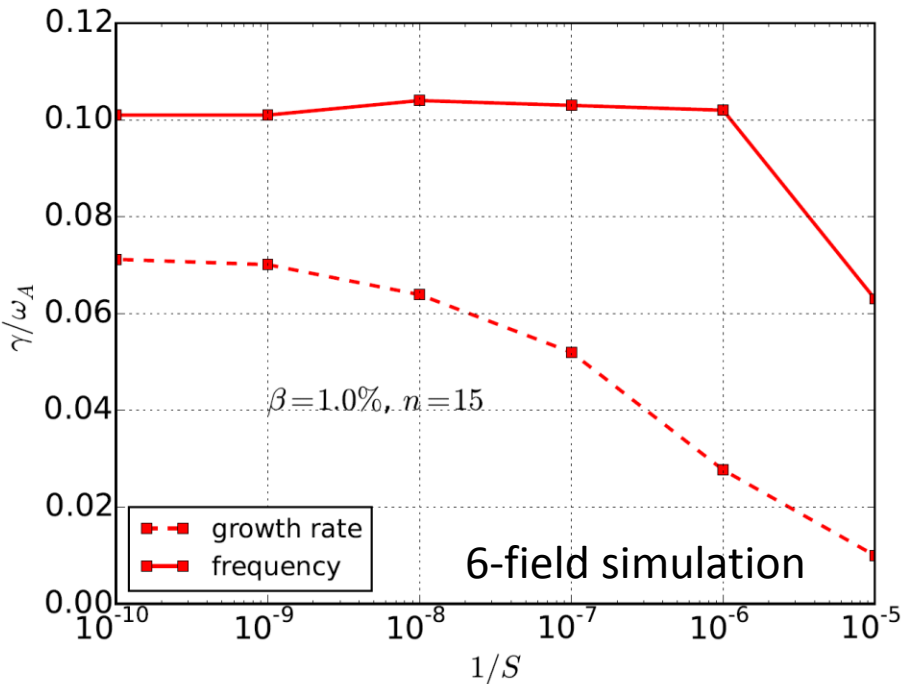
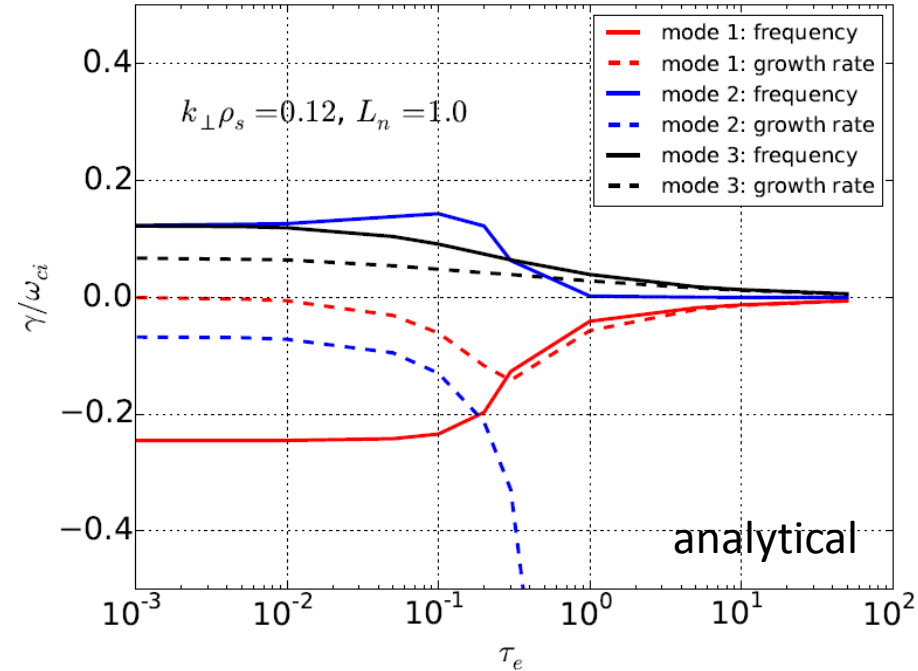
# Benchmark with drift Alfvén modes



- The dispersion relationship of drift Alfvén mode is:

$$\frac{c_s^2}{v_A^2} \frac{\omega^3}{k_{\parallel}^2} + i\tau_e \frac{k_{\perp}^2}{k_{\parallel}^2} \omega^2 - (1 + k_{\perp}^2)\omega + \frac{k_y}{L_n} = 0 \quad \tau_e = \frac{\nu_e m_e}{\omega_{ci} m_i}$$

- The analytical results are shown on left:



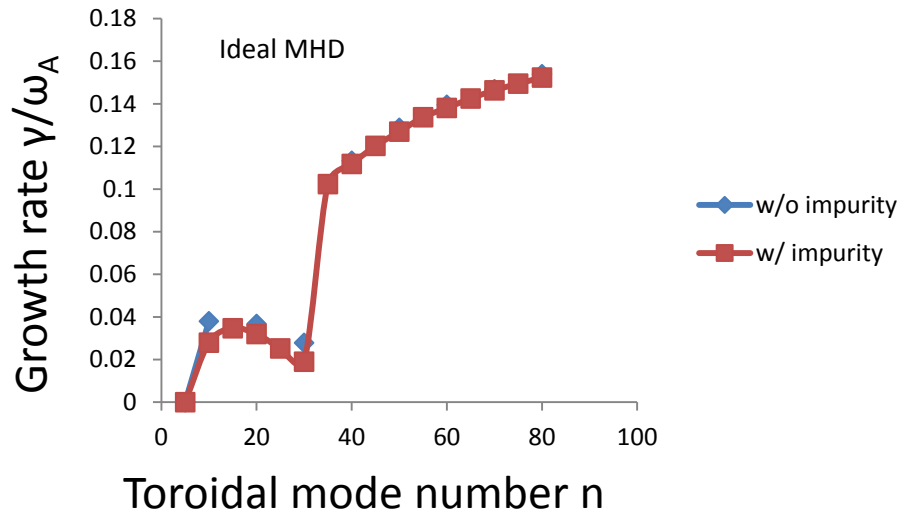
- Drift Alfvén mode is included in 6-field model under switch eHall.
- Within the similar parameters, 6-field model obtains the similar results on both growthrate and frequency for resistivity scan.



# The background impurity can stabilize the ballooning mode

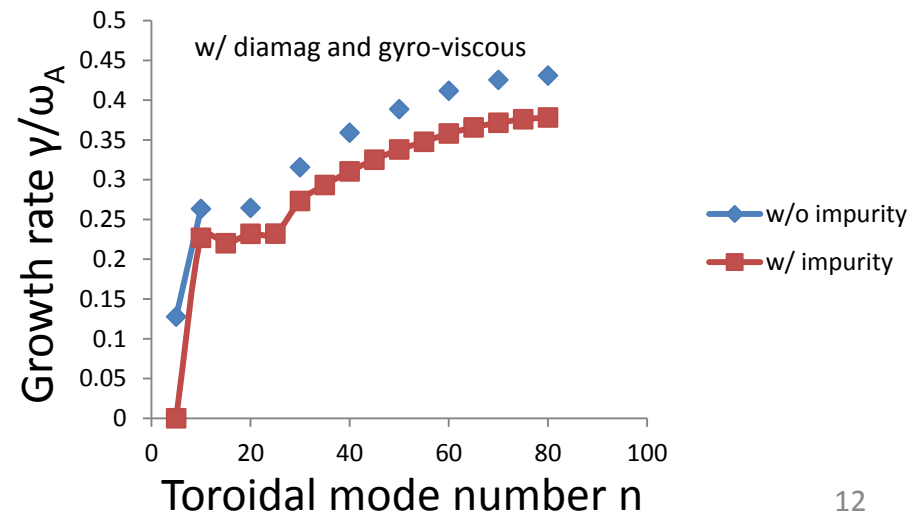


The effects of background impurity (carbon): can be treated as the change of mass density.



If the density profiles is kept unchanged  
➤ The effects of impurity: decreasing the low-n ballooning modes by  $\sim 14\%$ .

➤ If w/ both diamagnetic effects and gyro-viscosity, the growth rate for whole n is stabilized by impurity by  $\sim 12\%$ , more effectively.

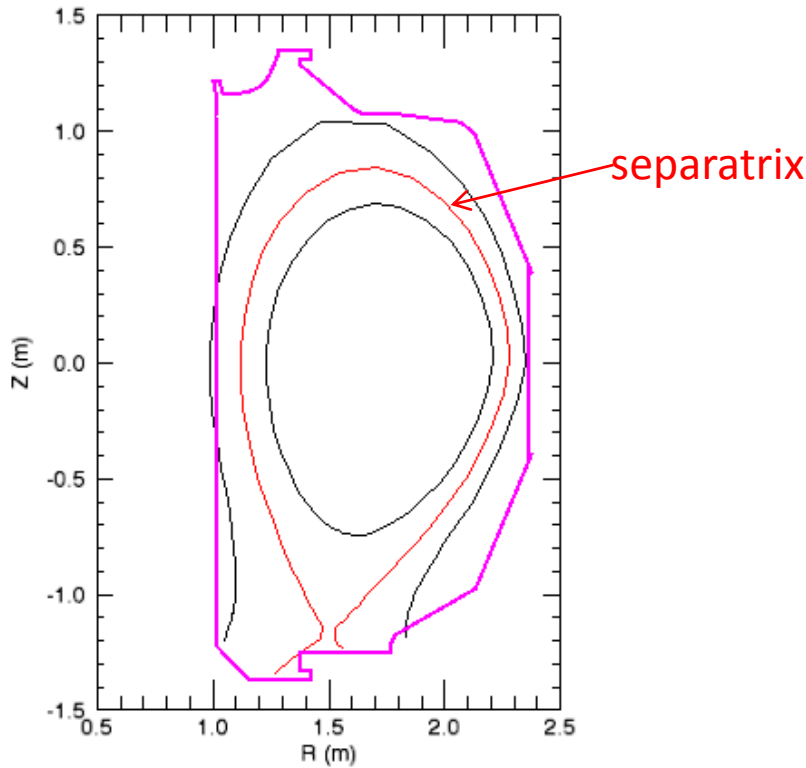




- Introduction of 6-field 2-fluid model
- Applications for divertor simulations
  - Transient heat flux simulations during ELM bursts on DIII-D
    - ◆ Kinetic modification on thermal conduction in pedestal
    - ◆ Validation with experiments
    - ◆ Study on the effects of magnetic flutter in parallel conduction
  - Transient particle flux simulations during ELM bursts on EAST
  - Summary for divertor simulations
- Demo for running 6-field



# Grid file used in linear simulation: DIIID H-mode discharge #144382 from 2500ms



The characteristic of #144382:

The lower single null geometry

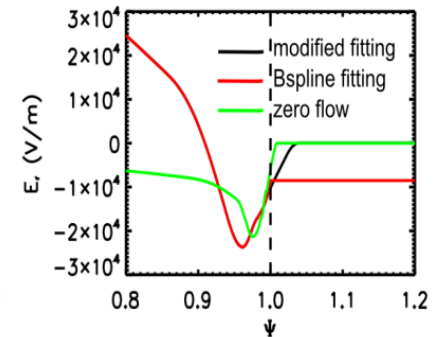
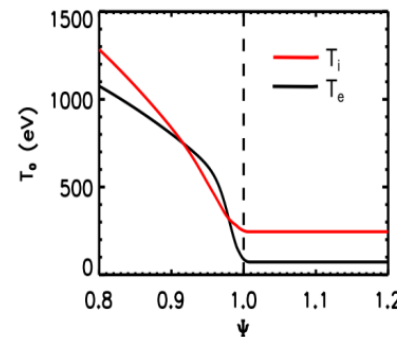
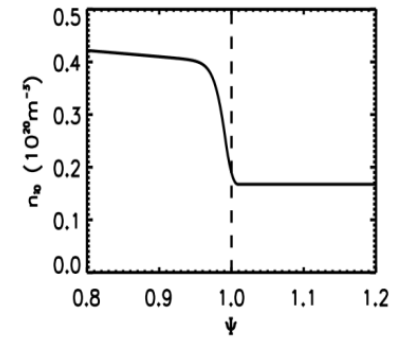
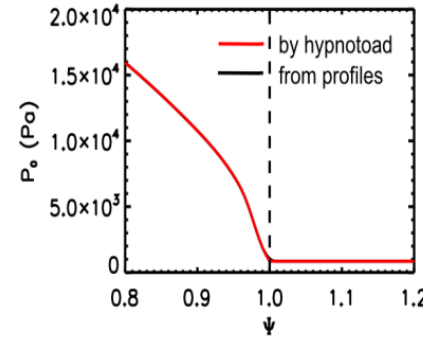
A low triangularity ( $\delta=0.35$ )

$\beta_N=1.9$

$I_p=1.16\text{MA}$

$f_{\text{ELM}}=150\text{Hz}$

$q_{95}=4.0$

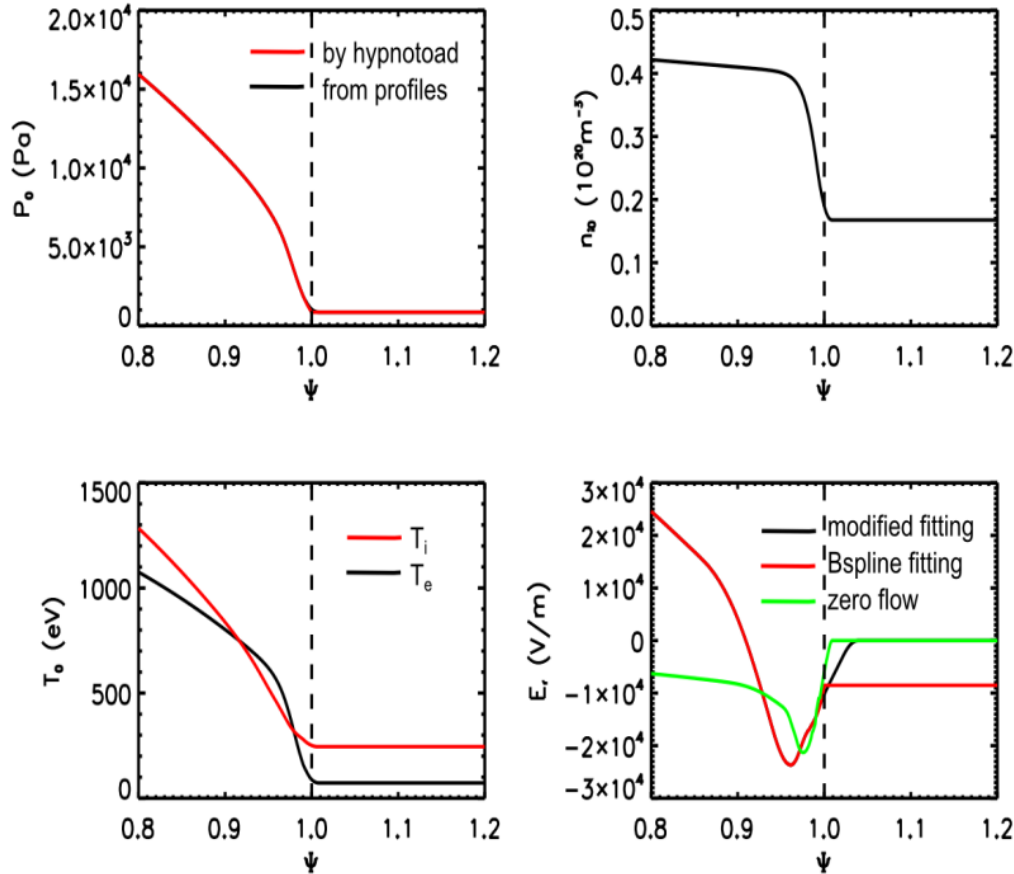


From experiments, this discharge is a small ELM crash event detected with multiple fast acquisition data chords in the pedestal, scrape-off layer (SOL) and divertor. This ELM produced a drop in the plasma stored energy of 2% (17 kJ from a 0.8 MJ plasma)\*.

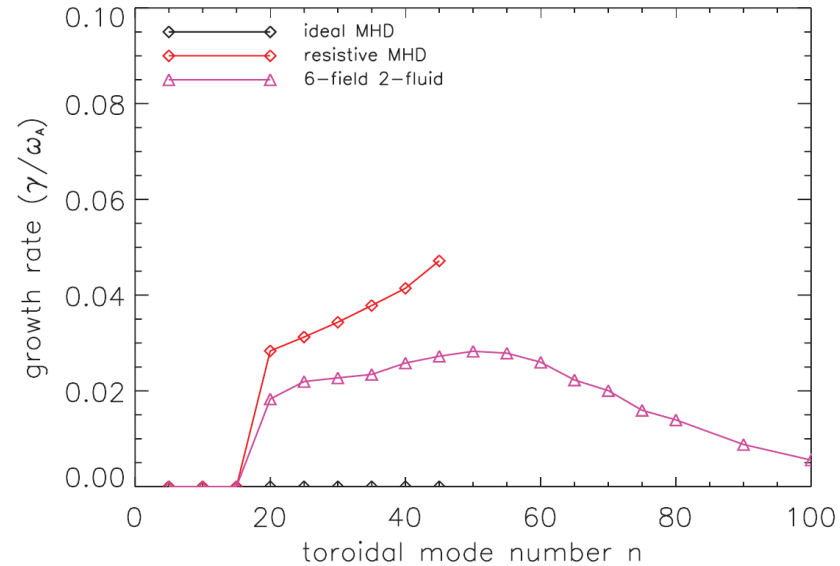
Profiles used in the simulations are derived from measurements.



# This discharge is ideal MHD stable, but resistive ballooning unstable



Profiles used in the simulations are derived from measurements.



Linear growth rate shows that #144382 is ideal stable for ideal peeling-ballooning mode. The instability is excited by resistive ballooning mode.



- Introductions
- Applications for divertor simulations
  - Transient heat flux simulations during ELM bursts on DIII-D
    - ◆ **Kinetic modification on thermal conduction in pedestal**
    - ◆ Validation with experiments
    - ◆ Study on the effects of magnetic flutter in parallel conduction
  - Transient particle flux simulations during ELM bursts on EAST
  - Summary for divertor simulations
- Demo for running 6-field



# Flux limiting coefficients describe the kinetic modification to Spitzer-Harm-Braginskii thermal conduction



$$\kappa_{\parallel i} = 3.9 n_i v_{th,i}^2 / \nu_i \quad \kappa_{\parallel e} = 3.2 n_e v_{th,e}^2 / \nu_e$$

$$\kappa_{fs,j} = n_j v_{th,j} q R_0 \alpha_j$$

Flux limiting coefficient  $\alpha_j$  represents the ratio of the Spitzer-Harm-Braginskii expression for parallel heat flux vs. free streaming flux.

$$\kappa_{eff,j} = \frac{\kappa_{\parallel j} \kappa_{fs,j}}{\kappa_{\parallel j} + \kappa_{fs,j}}$$

The typical range of  $\alpha_j$  is [0.03, 3.0]\*

How to determine the value of  $\alpha_j$ :

The free streaming limit:  $\alpha_j^{FS} = 0.8 - 1.0$

The sheath limit:  $\alpha_j^{SH} \simeq 2.5 \left( \frac{T_i}{T_e} + Z_i \right)^{\frac{1}{2}} \left( \frac{m_e}{m_i} \right)^{\frac{1}{2}} \simeq 0.058$   
 -- should be chosen for divertor simulations

For DIII-D #144382,  $\kappa_{\parallel ij}$  are dominated by the flux limited expression because of low collisionality, especially inside the separatrix.

$v_{e^*} = 0.127$  at  $\psi_N = 0.8$

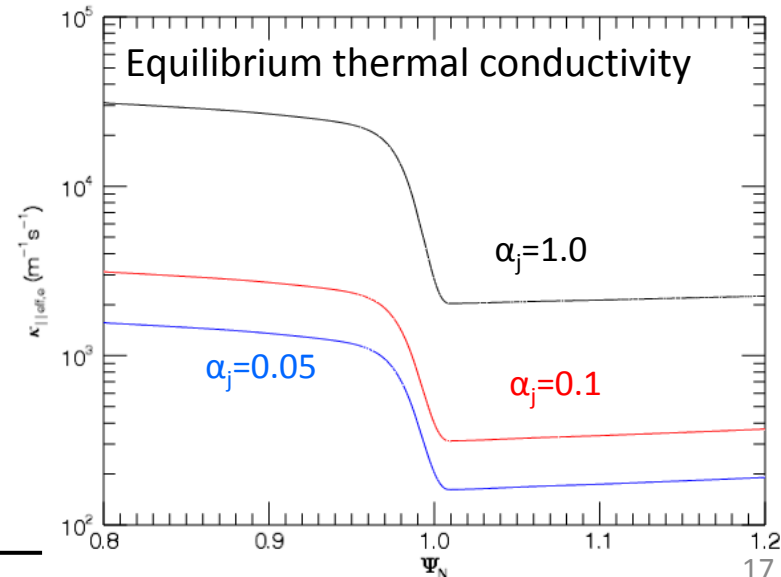
$v_{e^*} = 1.616$  at pressure gradient peak

Three different  $\alpha_j$  are discussed in our simulations:

$\alpha_j = 1.0$ : free streaming limit

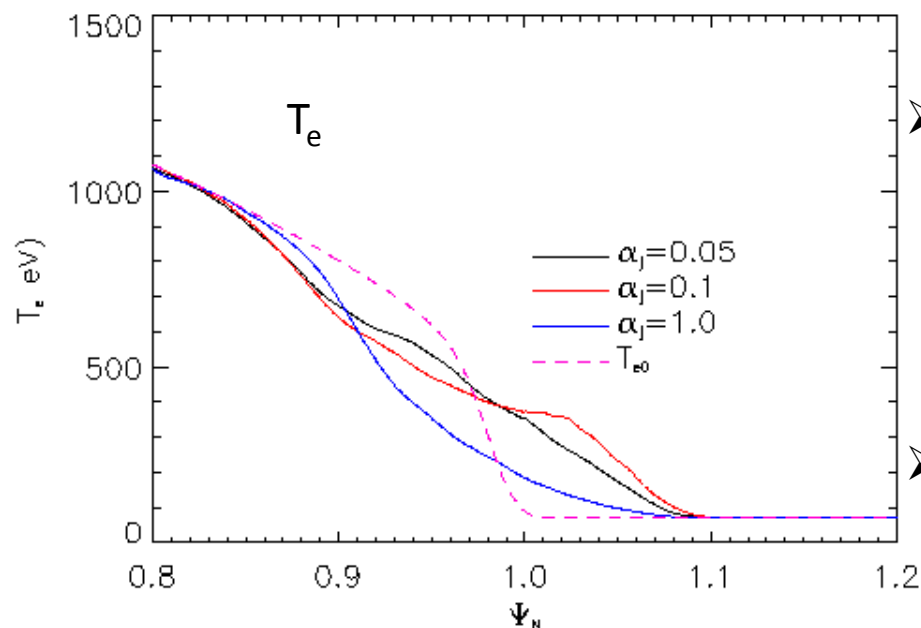
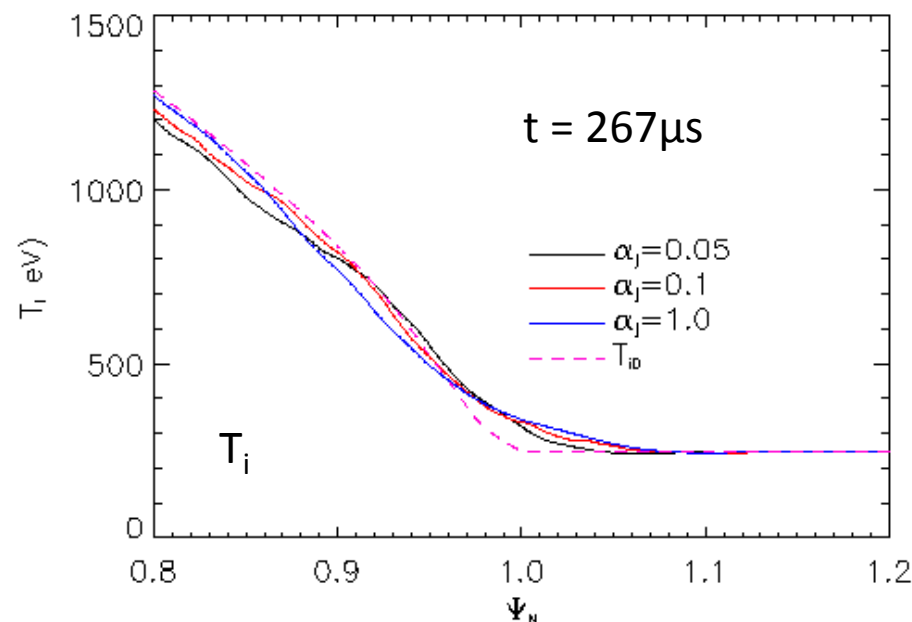
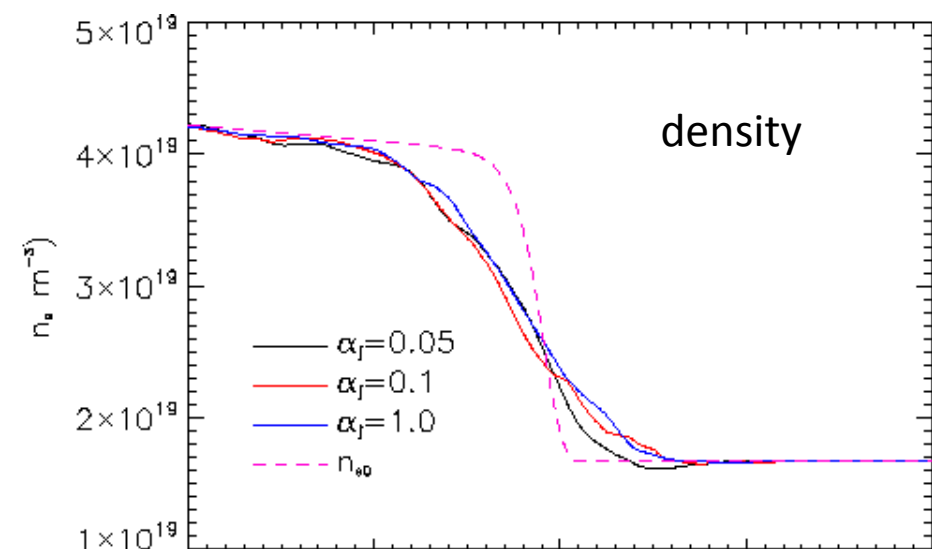
$\alpha_j = 0.05$ : sheath limit

$\alpha_j = 0.1$ : intermediate





# Thermal conduction stops the crash of the profile from peak gradient to inner boundary



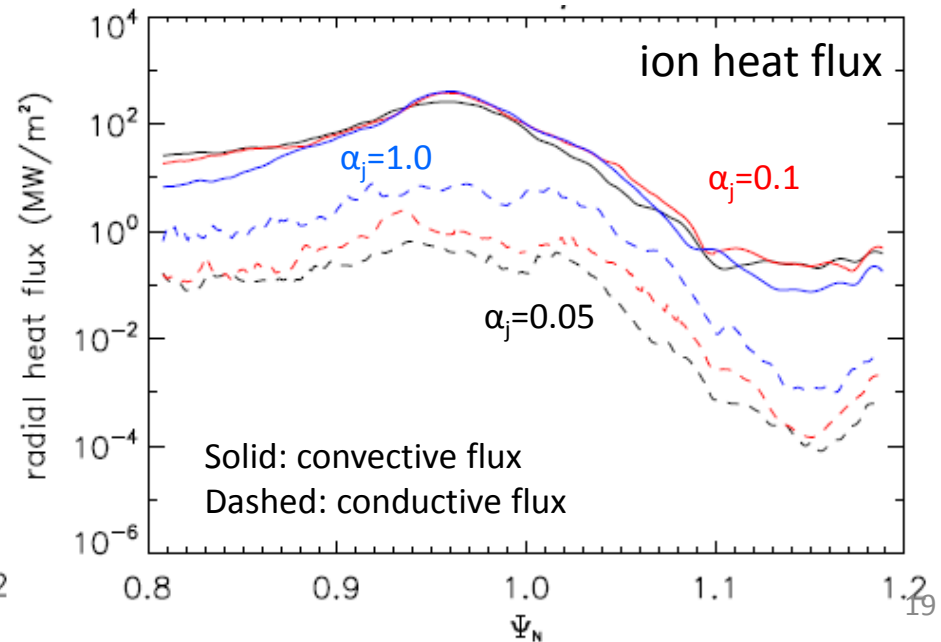
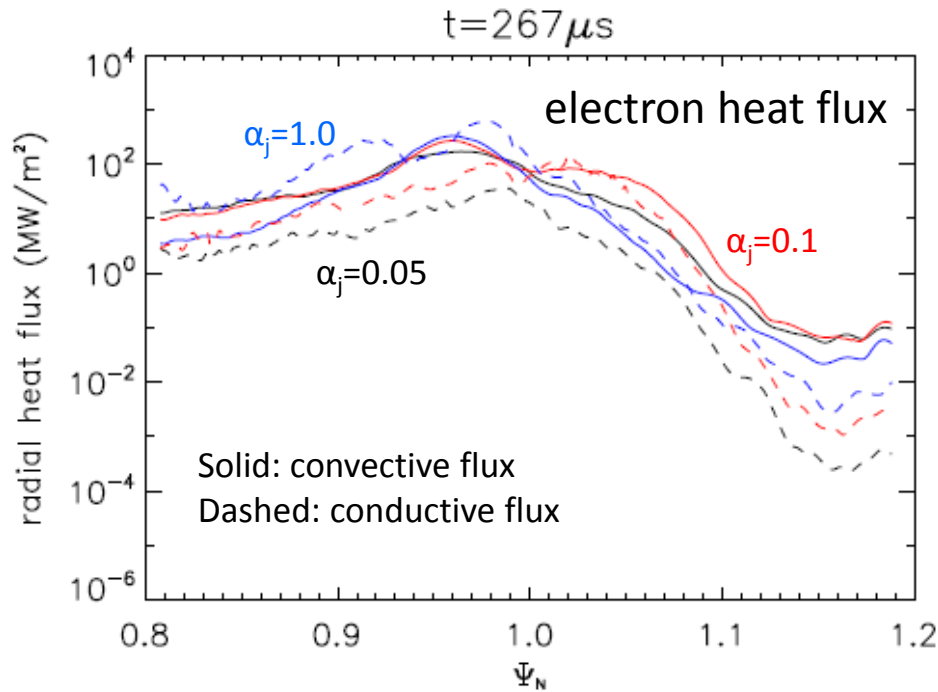
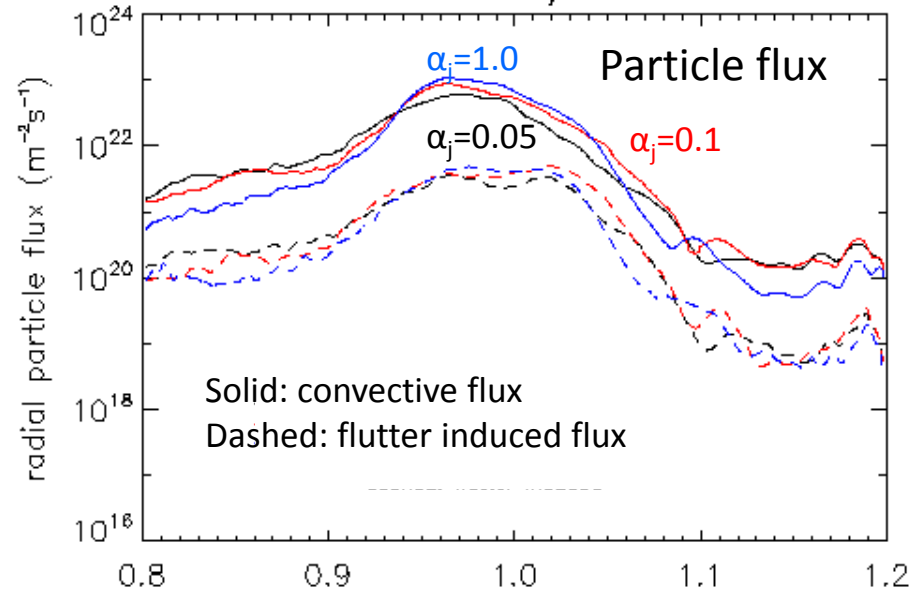
- The temperature profile is the most sensitively affected by  $\alpha_j$ .
  - Peak gradient region: larger  $\alpha_j$  leads to larger crash of profile
  - Pedestal top: larger  $\alpha_j$  leads to smaller differences from equilibrium
- The crash of the density profile is affected the least.



# Radial conductive flux is negatively correlated with $\alpha_j$ , while radial convective flux is positive correlated

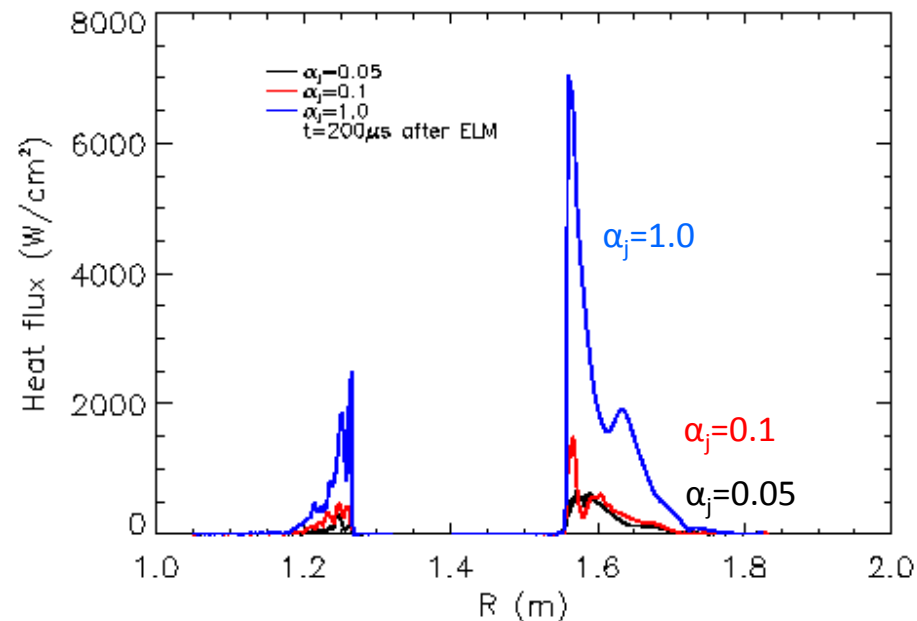
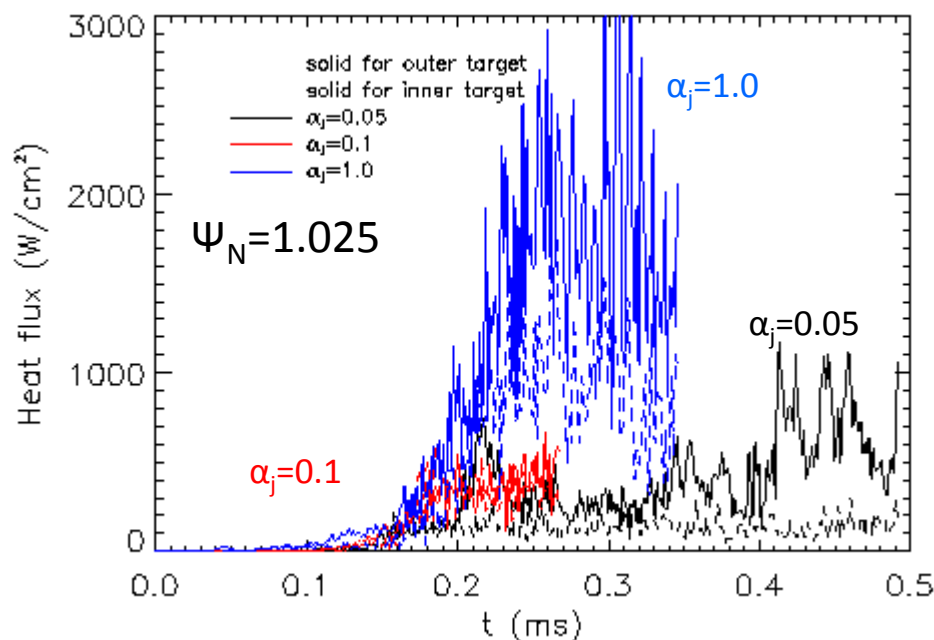


- The convective flux is the dominant component of the radial particle and ion heat fluxes.
- The larger  $\alpha_j$  leads to the larger radial fluxes, for both convective and conductive.
- For free streaming limit, the radial electron heat flux is almost averaged to convective and conductive components.
- The radial flux outside  $\psi_N \sim 1.05$  is 2 magnitude orders lower than that at the separatrix.





# The radial distributions of heat flux on targets are dramatically affected by $\alpha_j$

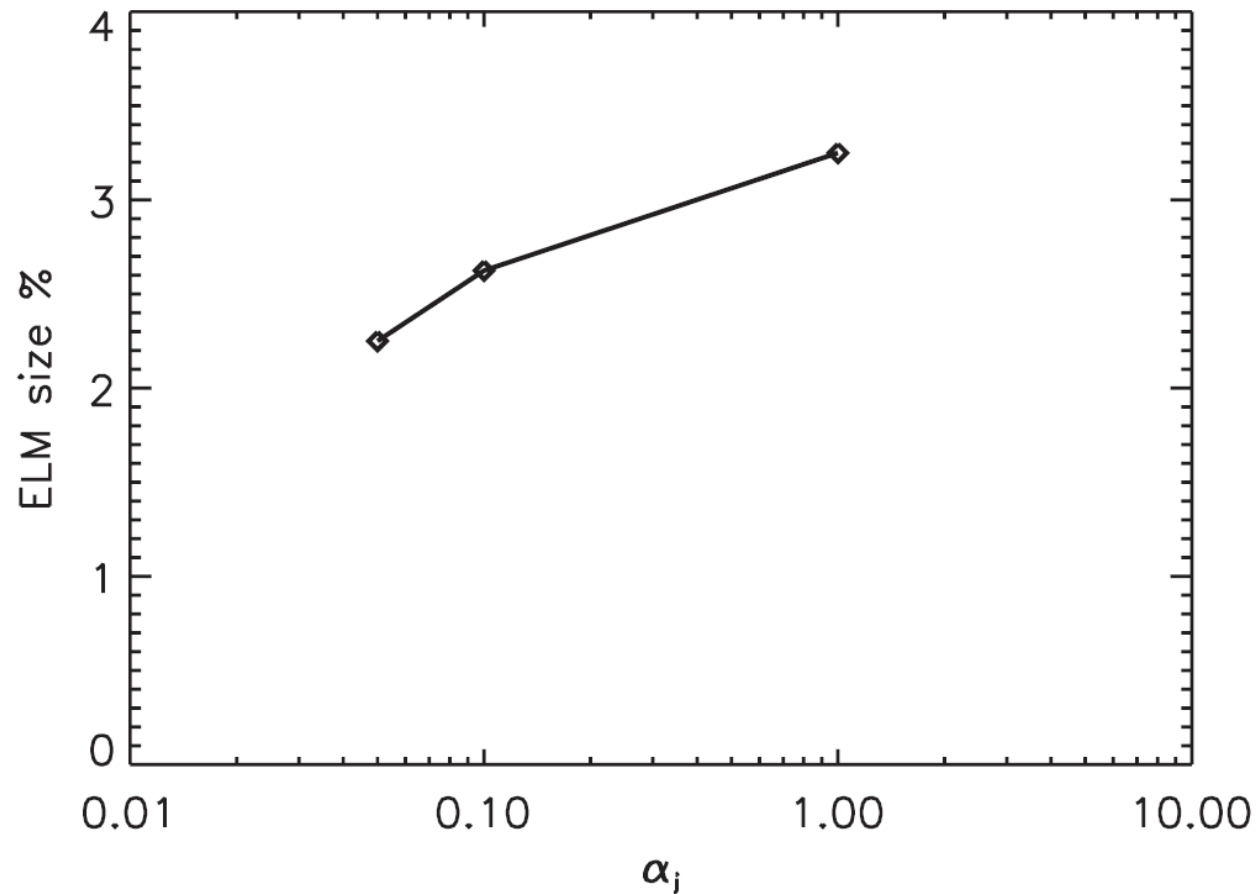


Dashed lines are inner target, solid curves are outer target.

- The amplitude of the heat flux on targets:
  - Outer target:  $q(\alpha_j=1):q(\alpha_j=0.1):q(\alpha_j=0.05) = 6.25873 : 1.37994 : 1$
  - Inner target:  $q(\alpha_j=1):q(\alpha_j=0.1):q(\alpha_j=0.05) = 6.31188 : 2.35807 : 1$
- The larger  $\alpha_j$  leads to wider expansion of the heat flux on targets.
- Compared to DIII-D diagnostics, the sheath limit of  $\alpha_j$  is the most reasonable coefficients to simulate the H-mode heat flux on divertor target.



# The sheath limit model for flux-limiting obtains ELM size close to the experiments



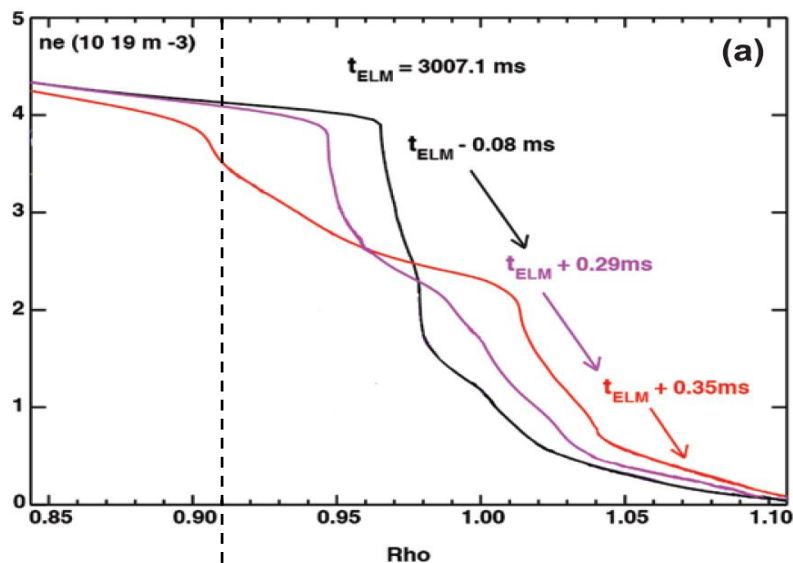
The simulated ELM size under sheath limit parallel conduction with  $\alpha_i=0.05$  is around **2.2%**, which is very close to the experimental measurement with **2\***.



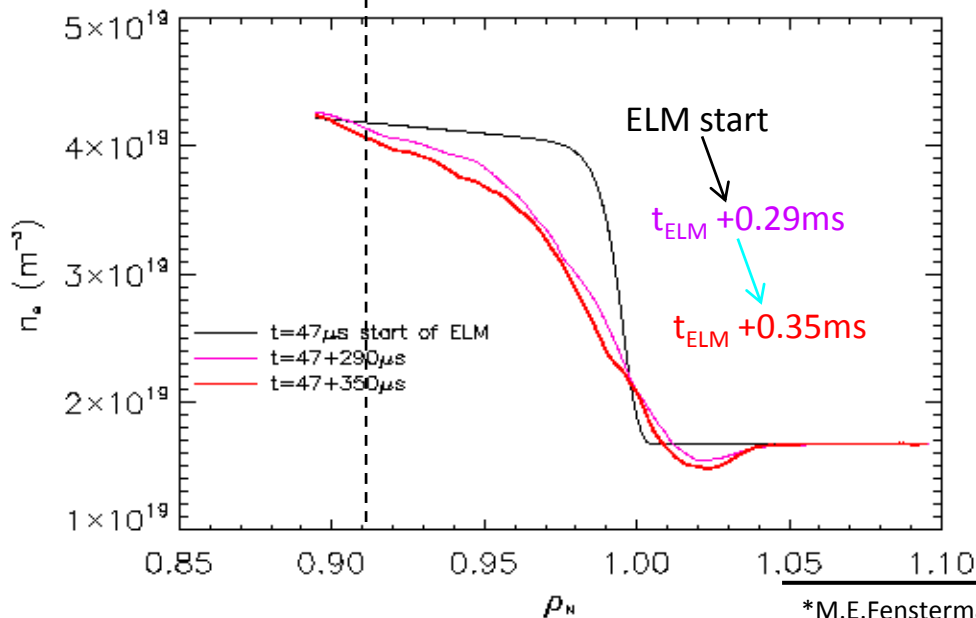
- Introductions
- Applications for divertor simulations
  - Transient heat flux simulations during ELM bursts on DIII-D
    - ◆ Kinetic modification on thermal conduction in pedestal
    - ◆ **Validation with experiments**
    - ◆ Study on the effects of magnetic flutter in parallel conduction
  - Transient particle flux simulations during ELM bursts on EAST
  - Summary for divertor simulations
- Demo for running 6-field



# The comparison of the density profiles between simulations and measurements



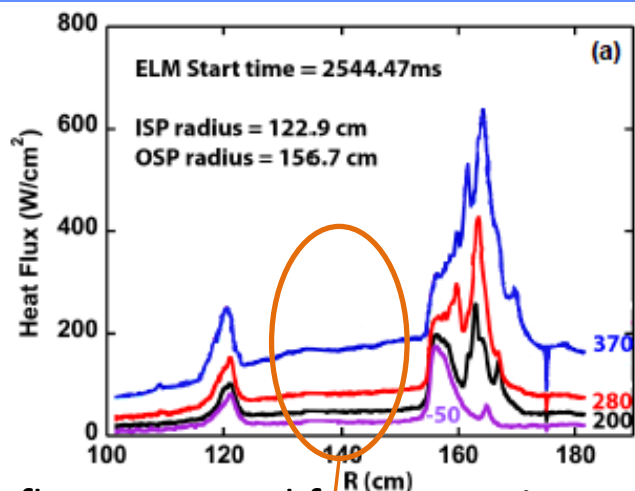
Measured from DIIID diagnostics.



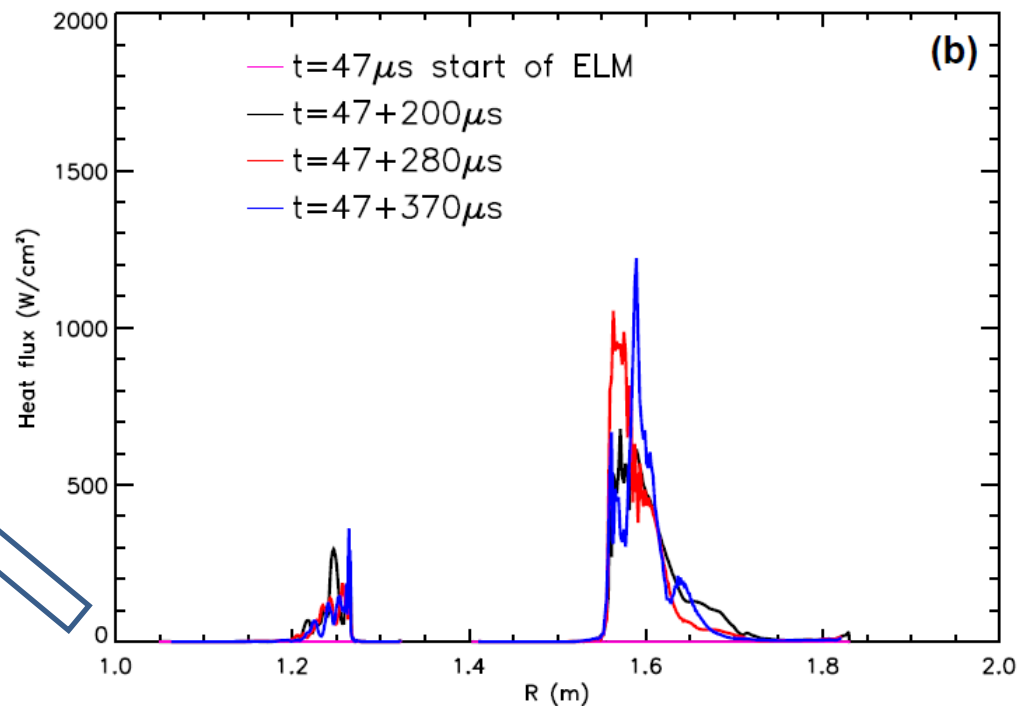
The simulations for density.

- The ELM crash event are well described by the simulation.
- The red curve shows the similar expansion of the density profile crash with the measurement at the same time.

# The comparison of the heat flux profiles between simulations and measurements



Heat flux measured from experiments\*.

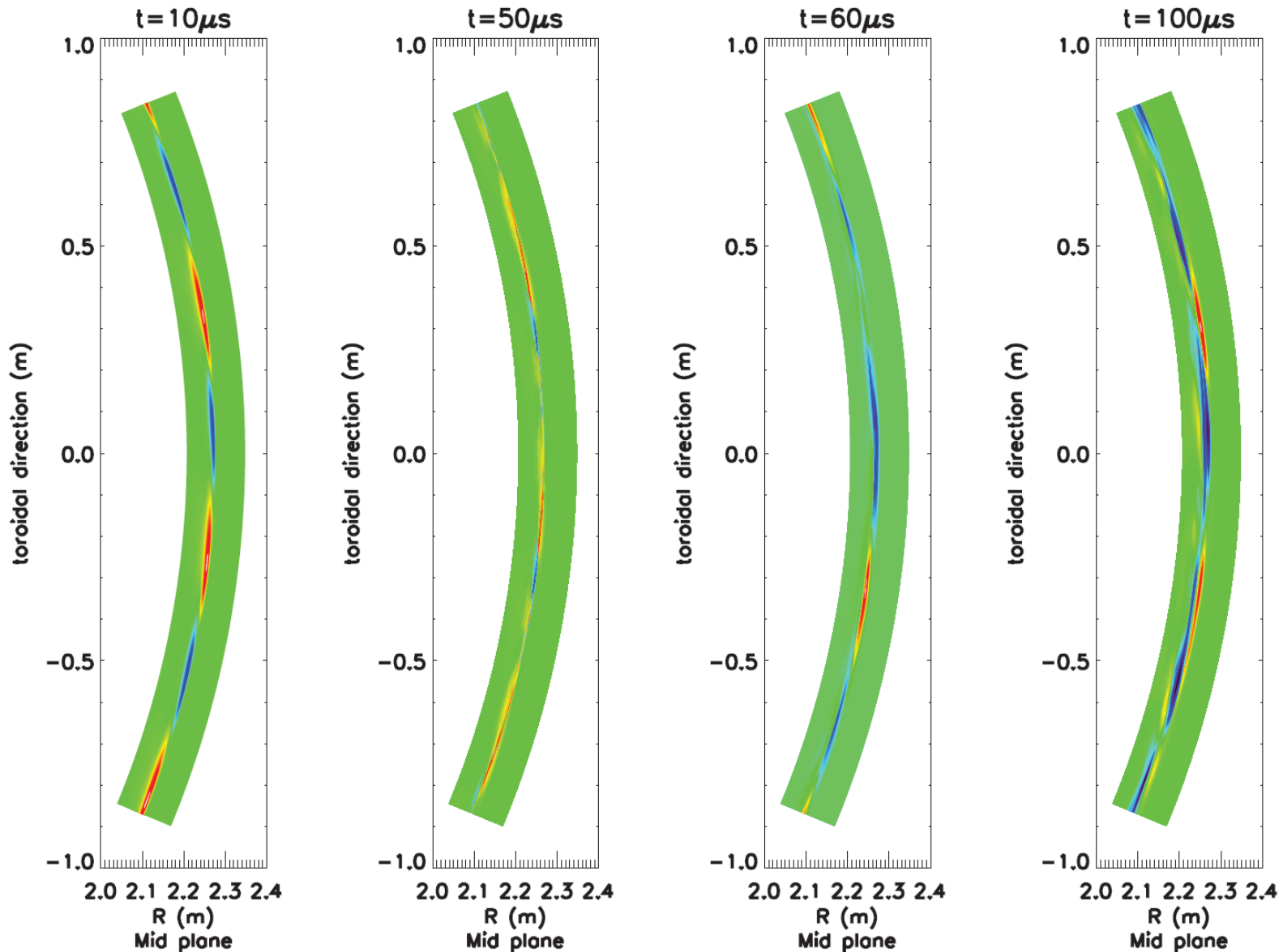


Due to reflections in the IRTV, which have been significantly reduced in the 2013 DIII-D campaign.

- Heat fluxes from simulations show the comparable expansion on targets.
- Compared to the measurement, the amplitude is 2x times larger due to the lack of radiation and recombination by neutrals and impurities.

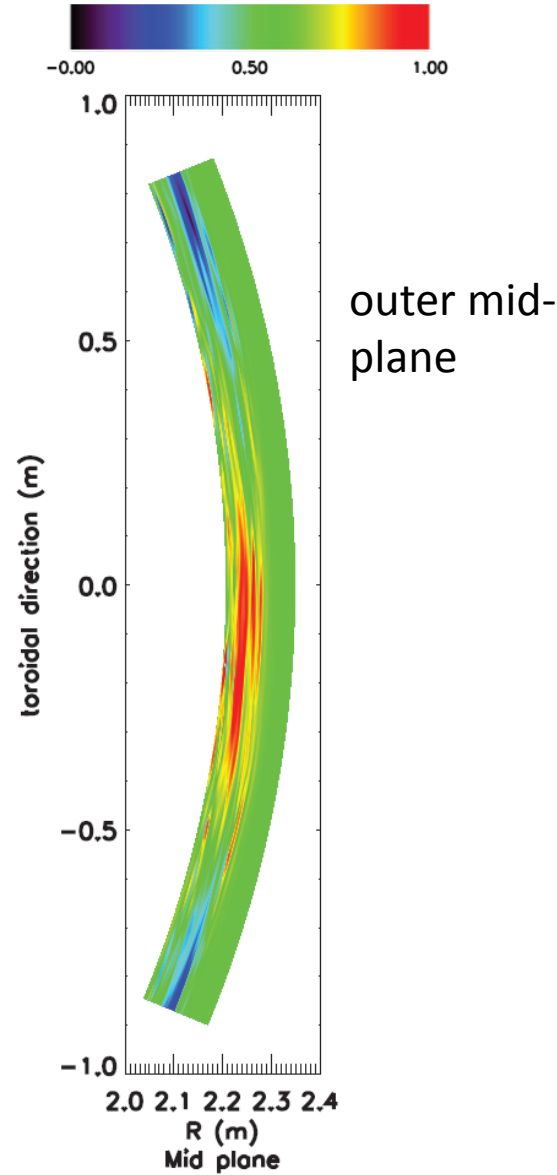
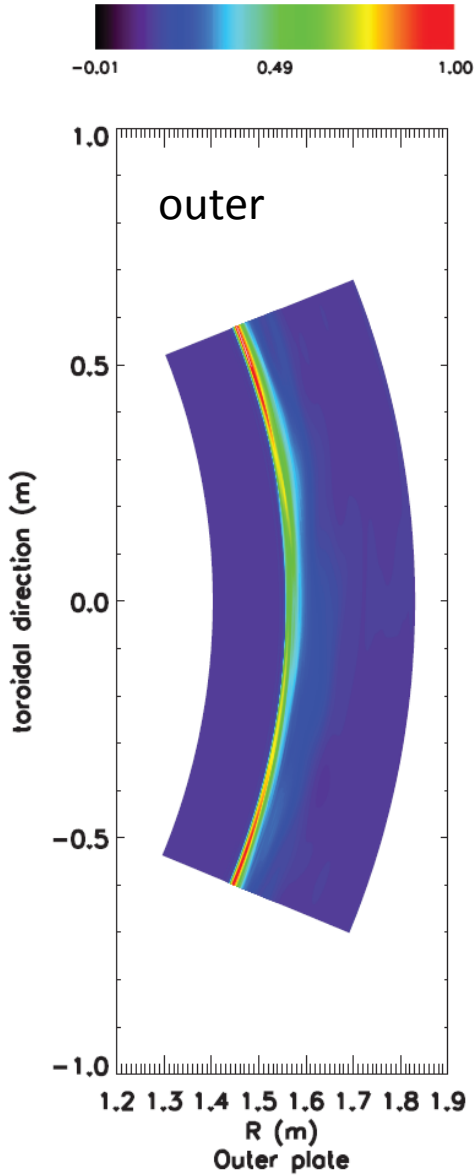
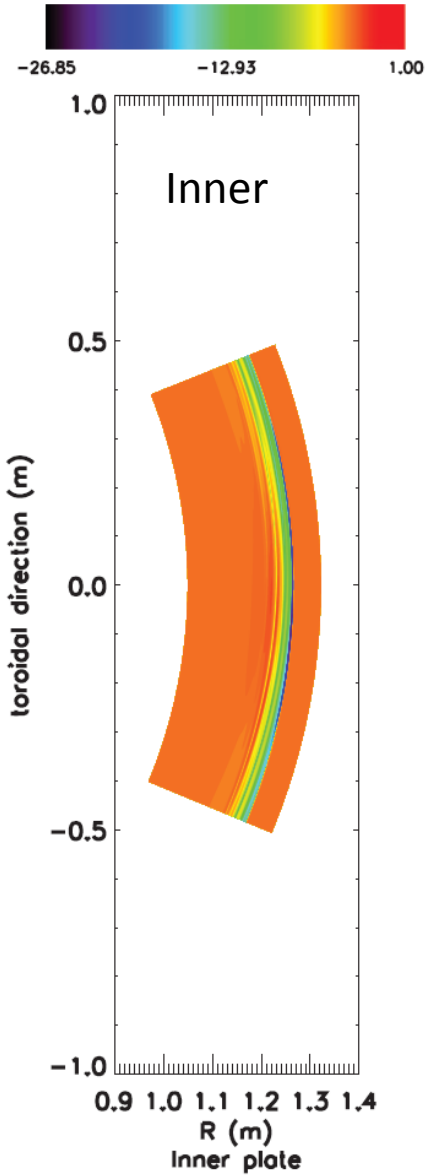


# The evolution of the toroidal structure of $T_e$ at outer mid-plane during the burst of ELM





# The heat flux distribution on the toroidal plane at $t = 400\mu\text{s}$





- Introductions
- Applications for divertor simulations
  - Transient heat flux simulations during ELM bursts on DIII-D
    - ◆ Kinetic modification on thermal conduction in pedestal
    - ◆ Validation with experiments
    - ◆ **Study on the effects of magnetic flutter in parallel conduction**
  - Transient particle flux simulations during ELM bursts on EAST
  - Summary for divertor simulations
- Demo for running 6-field

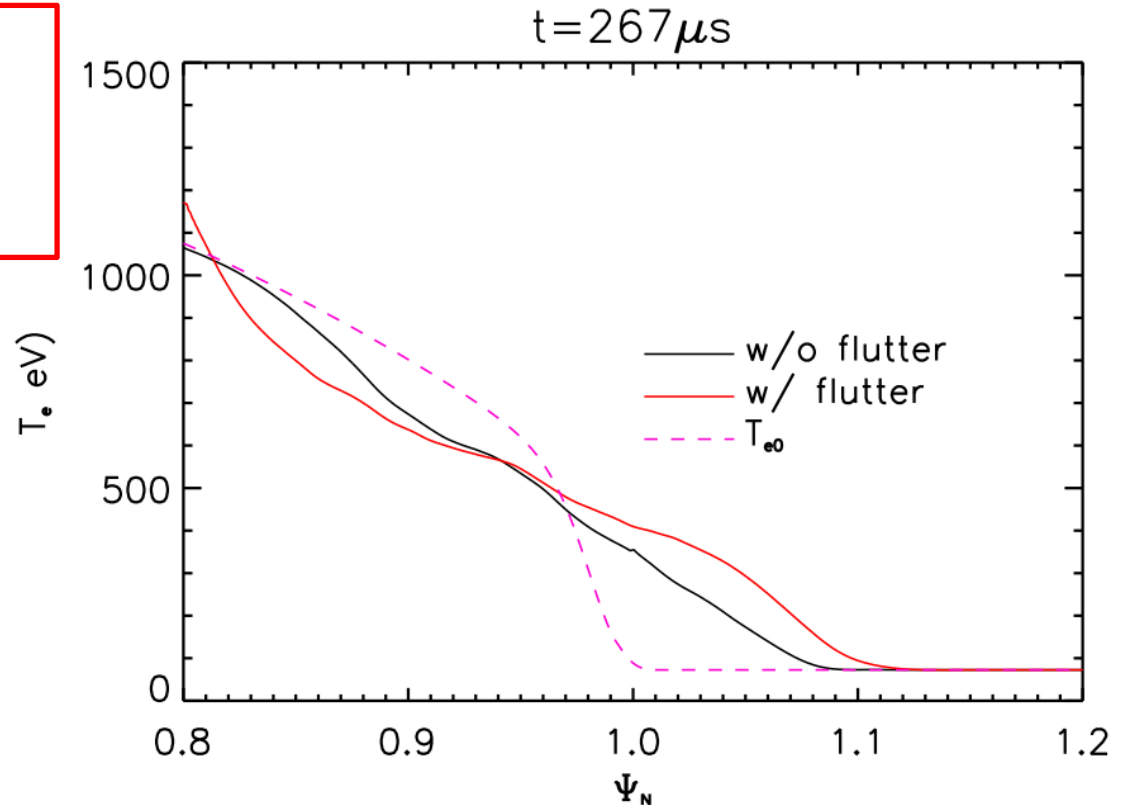


# Magnetic flutter in parallel thermal conduction



$$\nabla_{\parallel}(\kappa_{\parallel j} \nabla_{\parallel} T_j) = \nabla_{\parallel 0}(\kappa_{\parallel j} \nabla_{\parallel 0} T_j) + \mathbf{b}_0 \times \nabla \psi \cdot \nabla(\kappa_{\parallel j} \nabla_{\parallel 0} T_j) + \nabla_{\parallel 0}(\kappa_{\parallel j} \mathbf{b}_0 \times \nabla \psi \cdot \nabla T_j) + \mathbf{b}_0 \times \nabla \psi \cdot \nabla(\kappa_{\parallel j} \mathbf{b}_0 \times \nabla \psi \cdot \nabla T_j).$$

The magnetic flutter induced thermal conduction. They can enhance the radial transport in pedestal and SOL.

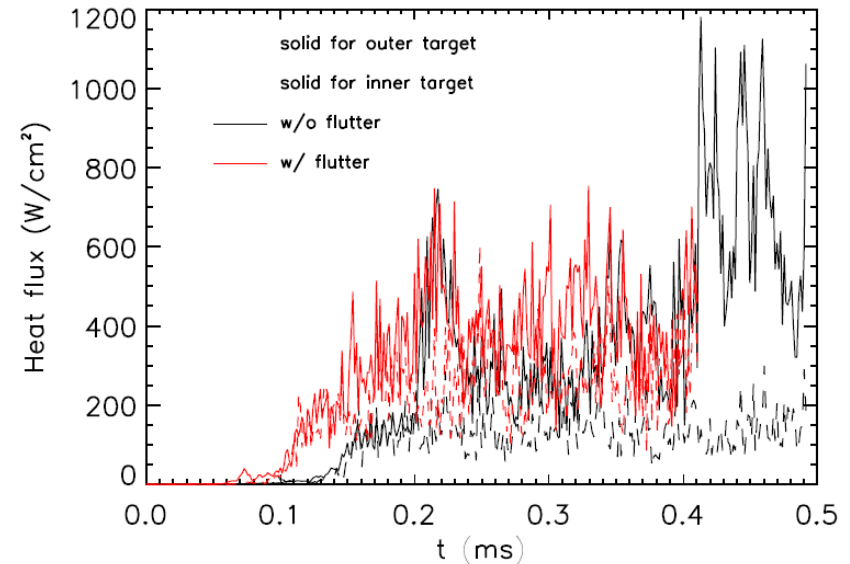
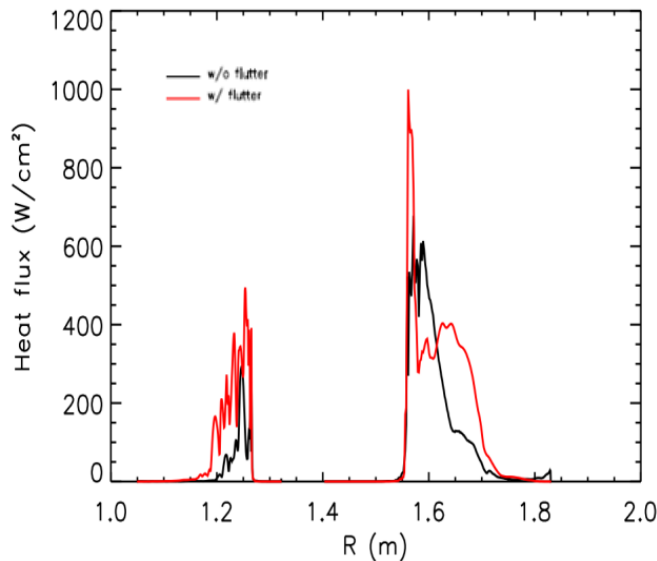
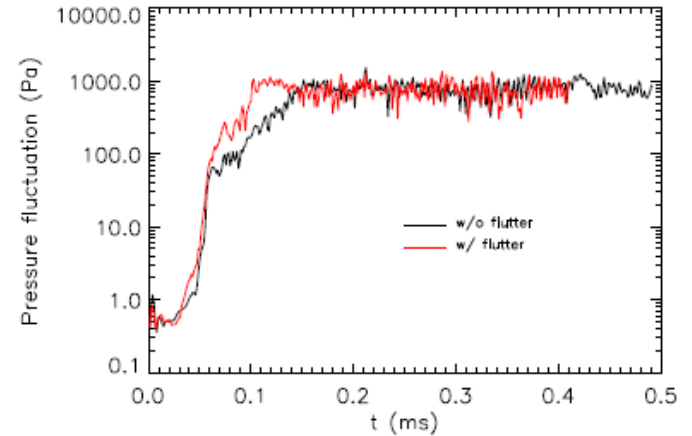




# The magnetic flutter enhance radial transport, then leads to larger Energy loss and heat flux



- More energy loss is due to magnetic flutter.
- At the linear phase, the growing of the perturbation is seldom affected.



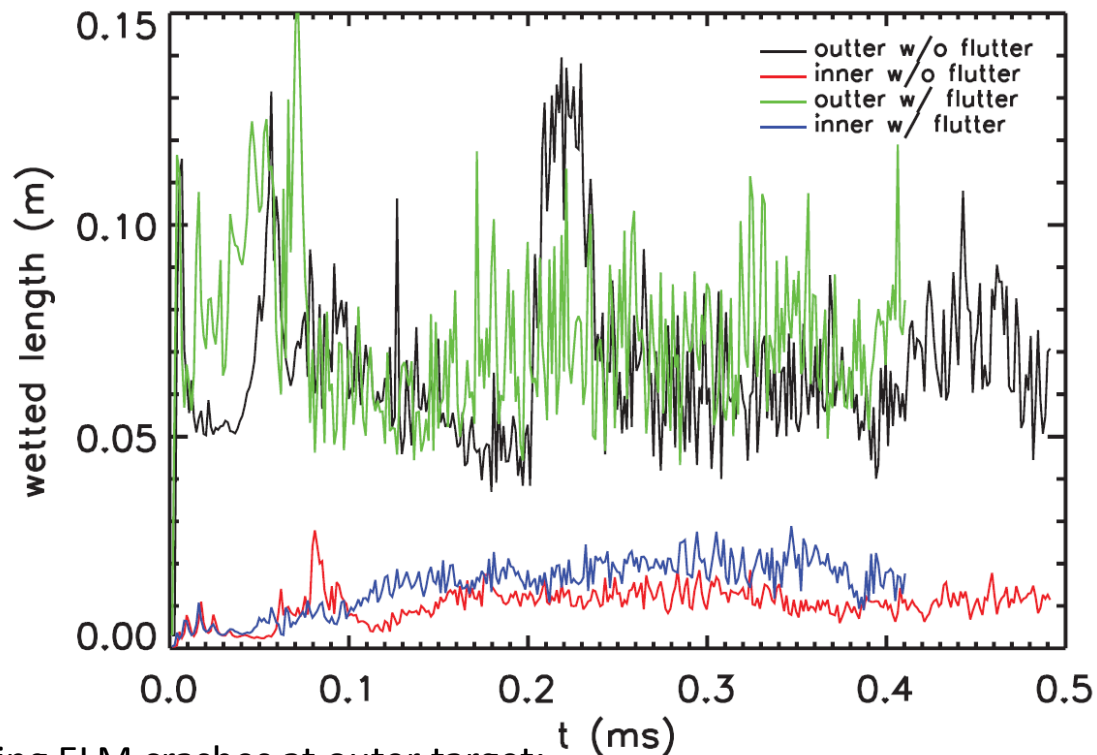
- Wider spreading of heat flux to targets, but larger peak value.
- Less difference between inner and outer targets with flutter.



# Magnetic flutter terms are able to broaden wetted length especially at the inner target



Wetted length: 
$$\lambda_w = \frac{\int q(t) dA}{2\pi R q_{\max}(t)}$$



During ELM crashes at outer target:

- $\lambda_w$  is broadened by 2.7 times due to the burst of ELM w/o flutter.
- $\lambda_w$  is broadened by 1.6 times due to the burst of ELM w/ flutter.

After t=0.1ms,

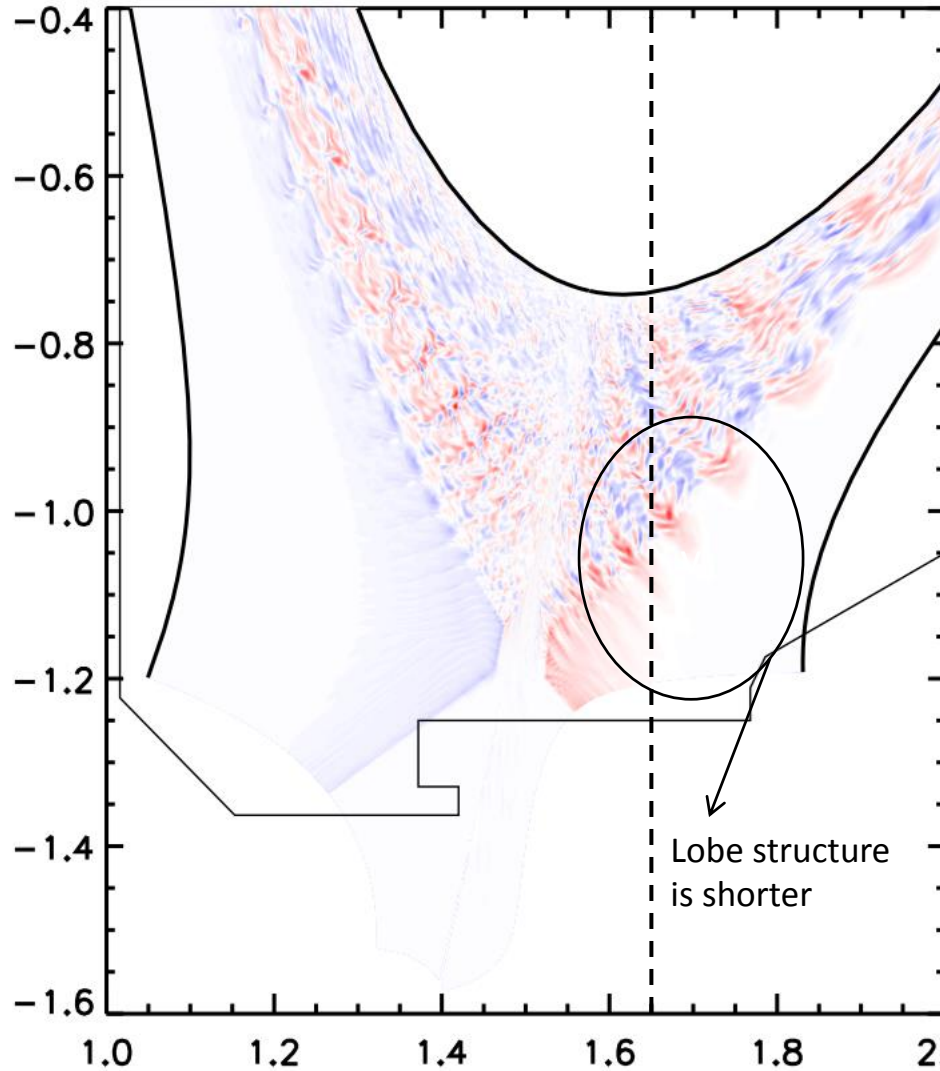
- At inner targets, flutter increases the width of the heat flux by ~50%.
- At outerer targets, the width is increased by ~6%.



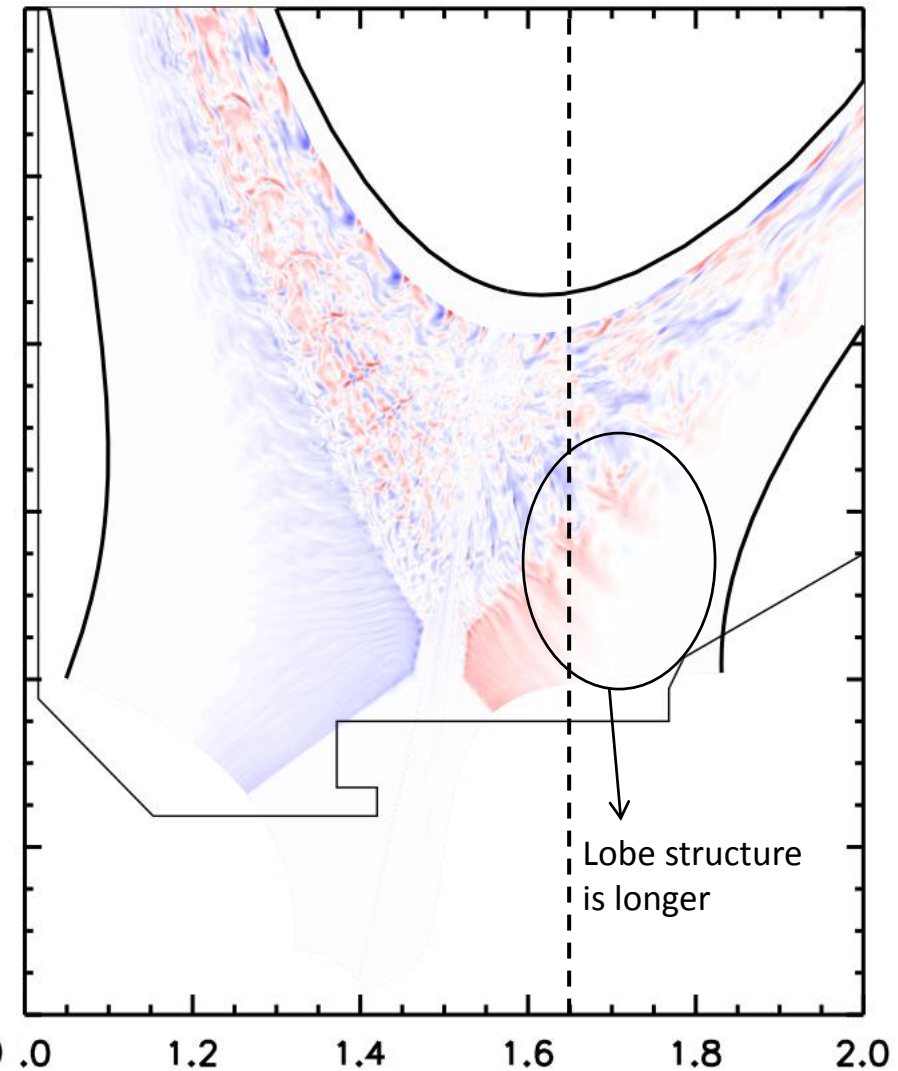
# The magnetic flutter terms are able to generate longer and wider lobe structures near the outer target



w/o flutter



w/ flutter

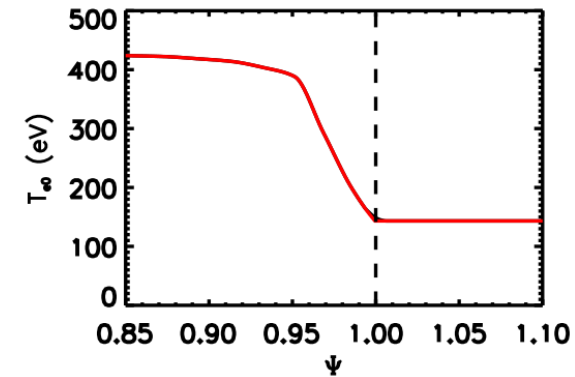
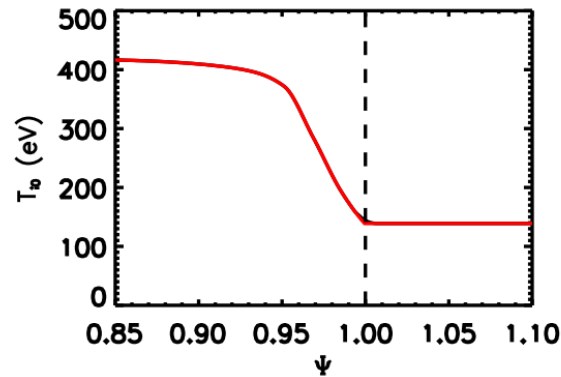
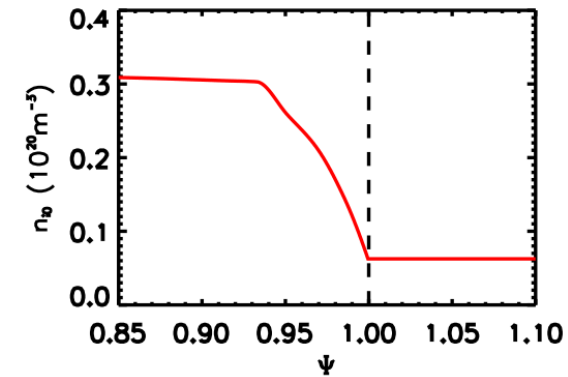
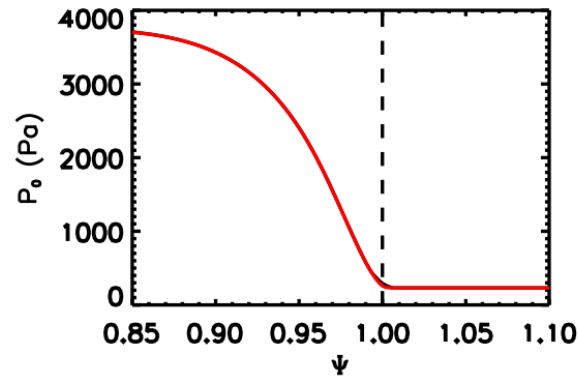
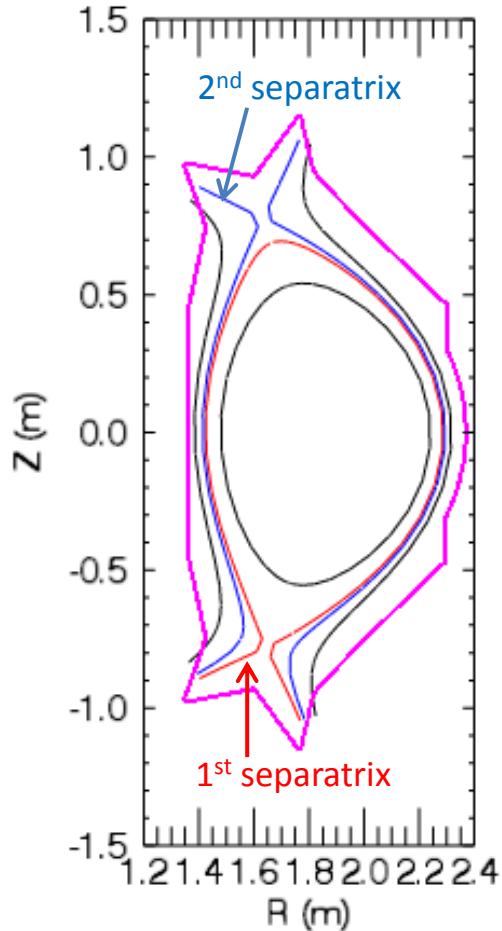




- Introductions
- Applications for divertor simulations
  - Transient heat flux simulations during ELM bursts on DIII-D
    - ◆ Kinetic modification on thermal conduction in pedestal
    - ◆ Validation with experiments
    - ◆ Study on the effects of magnetic flutter in parallel conduction
  - **Transient particle flux simulations during ELM bursts on EAST**
  - Summary for divertor simulations
- Demo for running 6-field



# The setup of EAST simulations

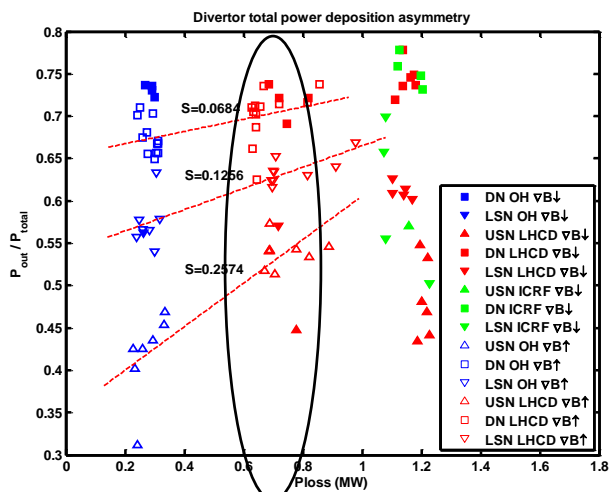


The simulation domain prepared for our simulations. It is based on EAST ELMy H-mode discharge 38300 at 3000ms.

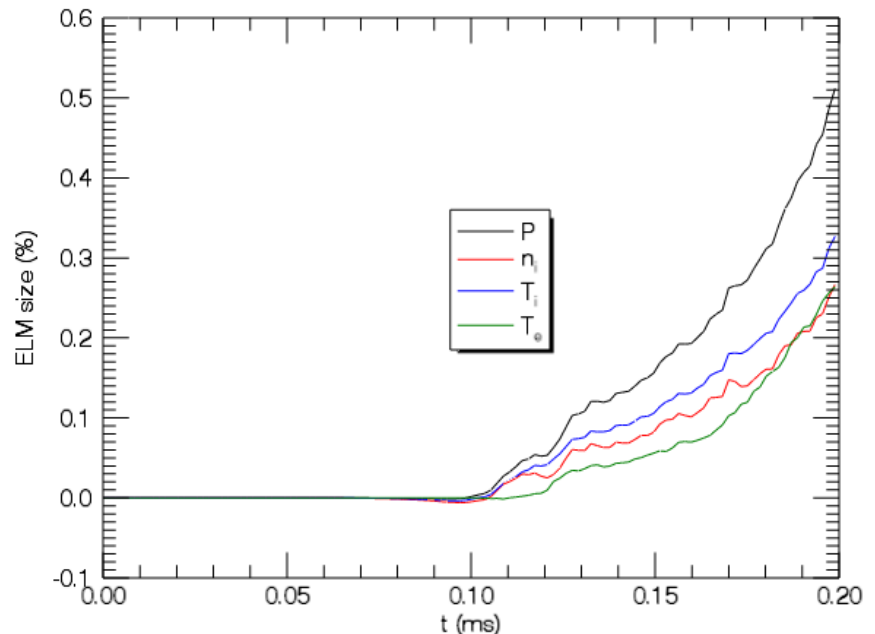
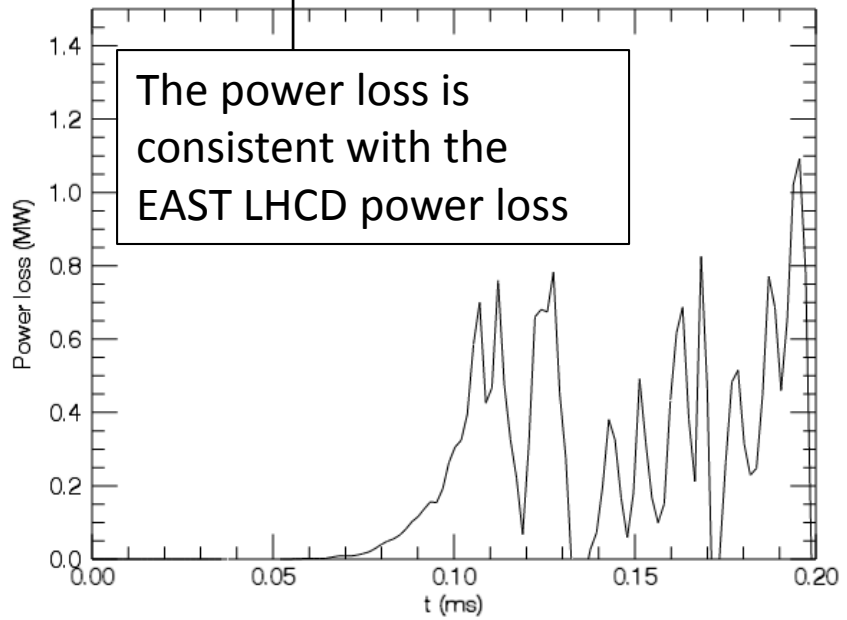
The fitted pressure profile, measures  $T_e$  and  $T_i$  are used as the input of simulations.



# Energy loss shows a small ELM event for this discharge

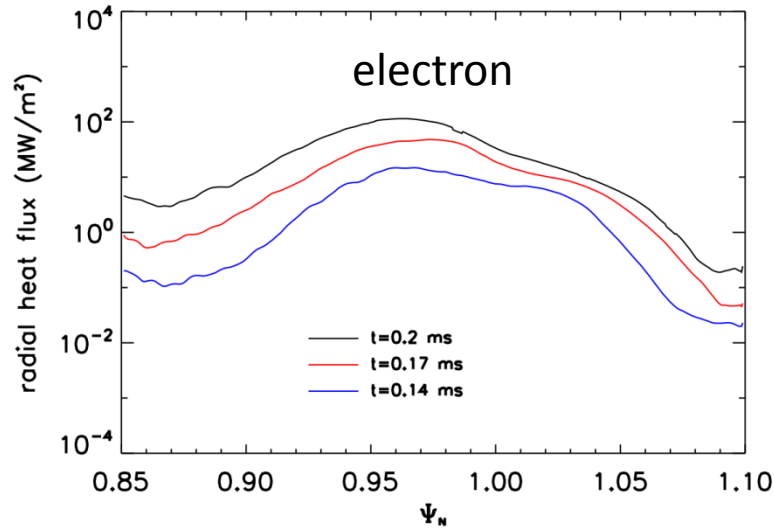
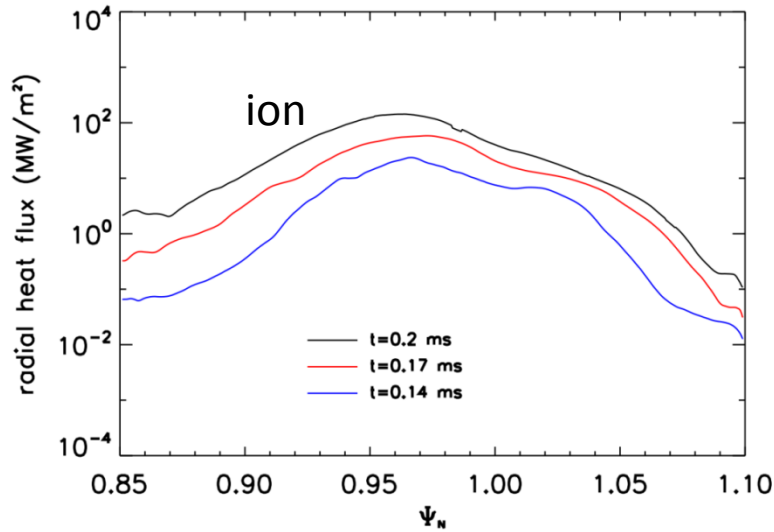


- The energy loss during the ELM is around 260J and ELM size is around 0.5%.
- The power loss is around 0.8MW, which is consistent with
- At this point, the ELM size is mainly contributed by the energy loss of ions.
- The energy loss of electrons are increasing and exceeds the particle loss of ions.

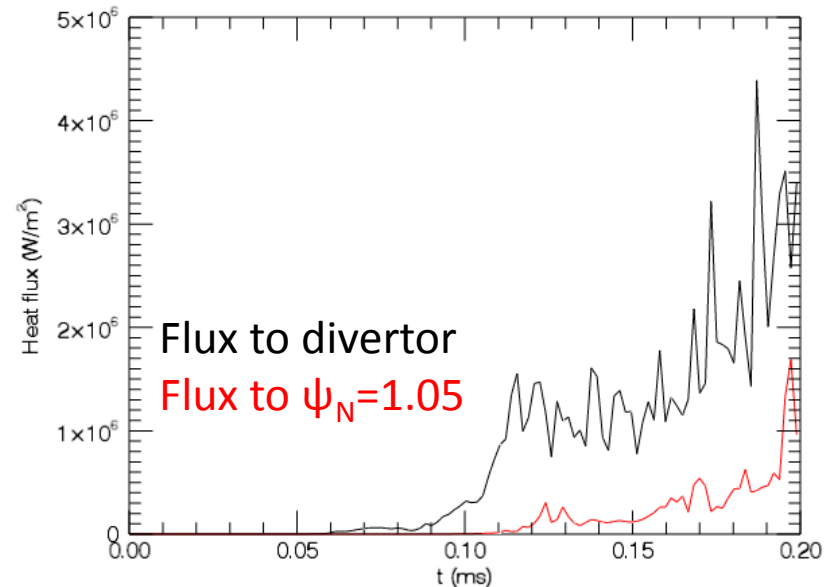




# The radial heat fluxes get faster increased outside the separatrix

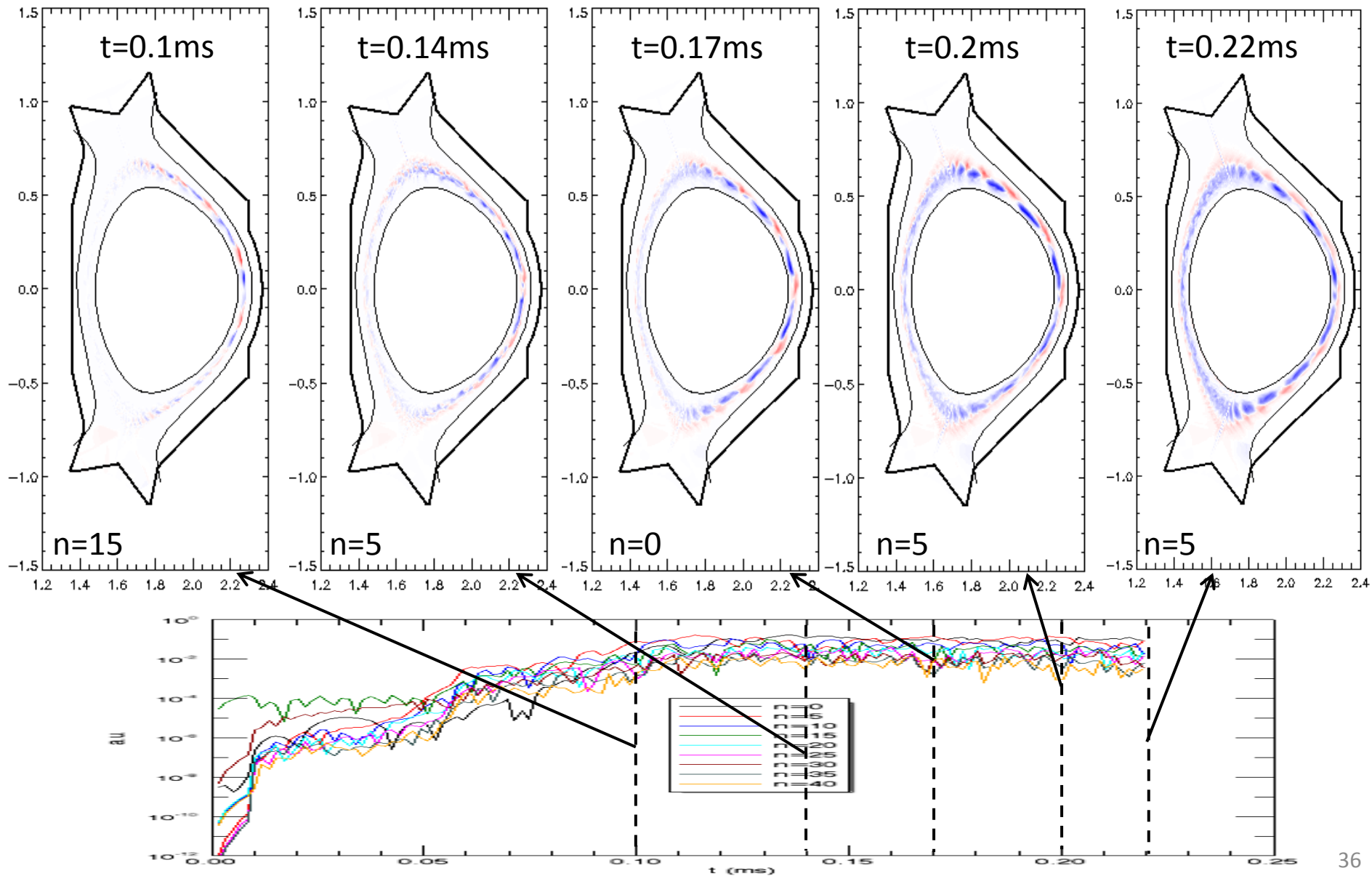


- The peak of the radial heat fluxes are just changed by 1 order of magnitude during the time from 0.14ms to 0.2ms.
- The outside of the separatrix are increased by nearly 2 orders of magnitude.
- This faster increase of the fluxes leads to the jump of the energy loss on walls.
- The energy loss on targets does not show the ELM burst event, because it will take  $L_c/v_{th} \sim 0.06$ ms to reach the divertors.



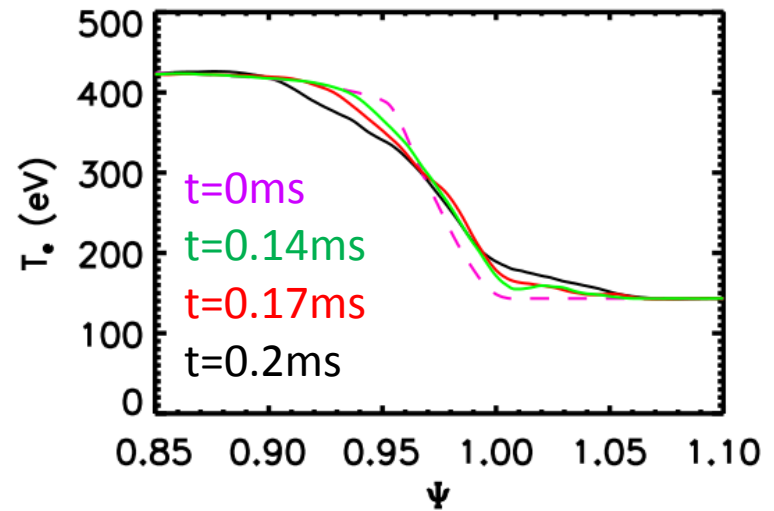
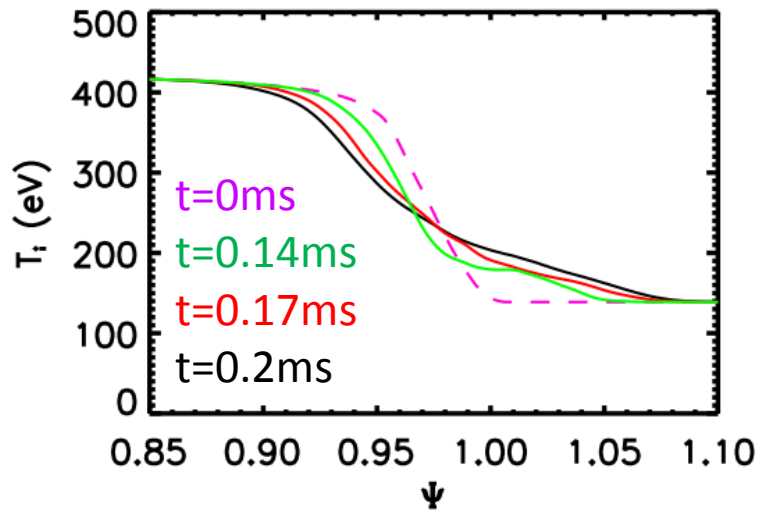
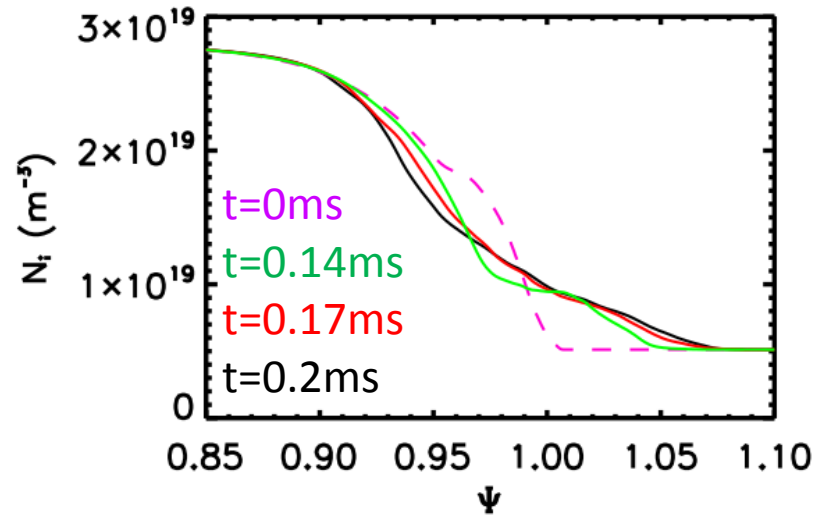
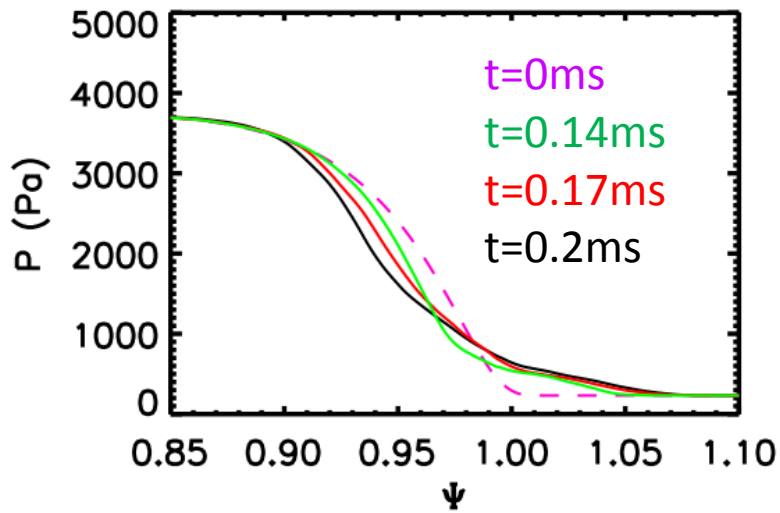


# The nonlinear filaments are determined by the dominant mode $n=5$ , which leads to the ELM burst



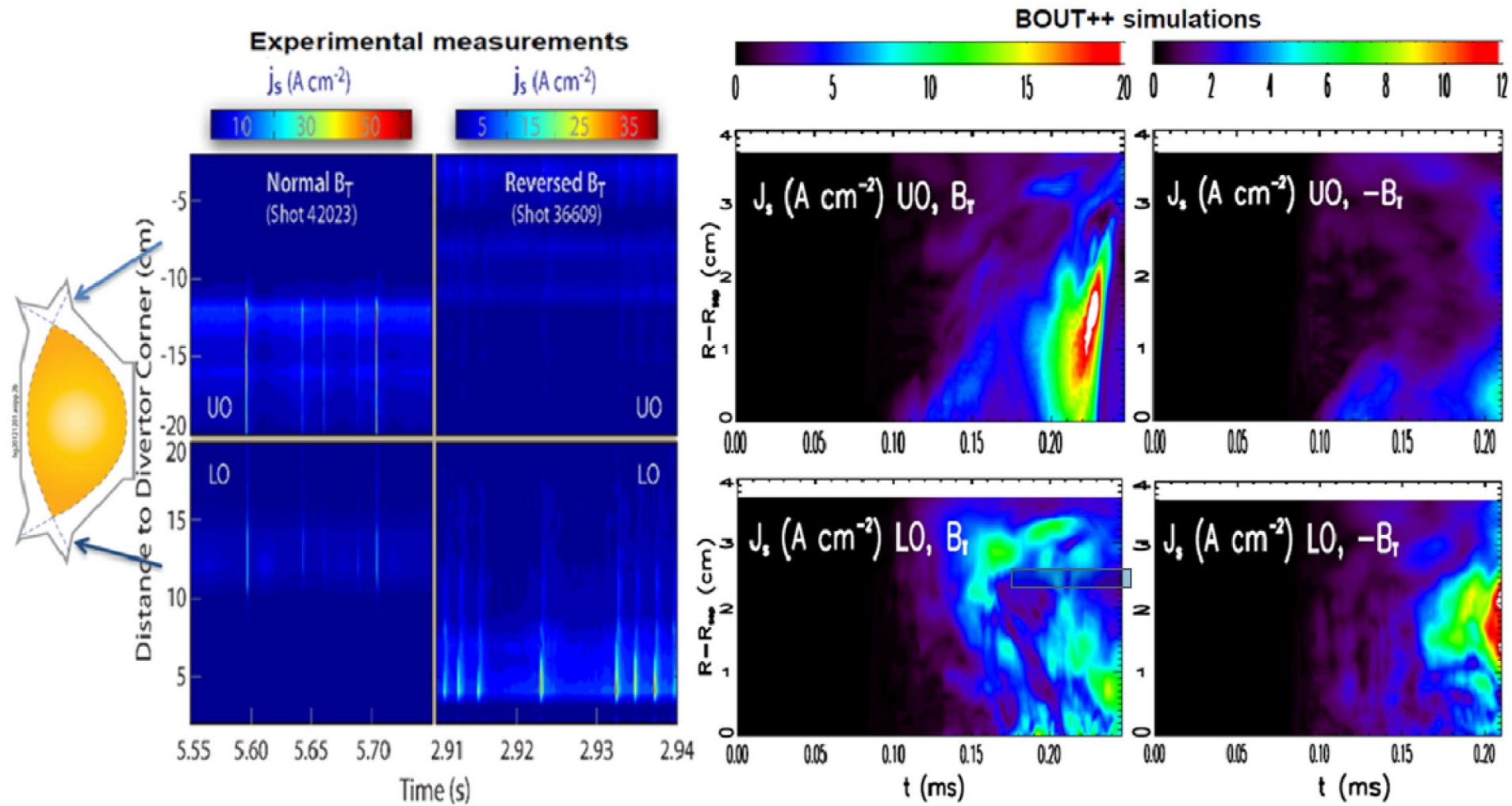


# The profiles are keeping relaxed during the ELM burst





# Particle flux distributions on upper and lower divertor targets are computed by 6-field model



Normal  $B_T$ : more particle flux on upper outer target

Reversed  $B_T$ : more particle flux on lower outer target



# Heat fluxes on upper and lower targets show the similar amplitudes

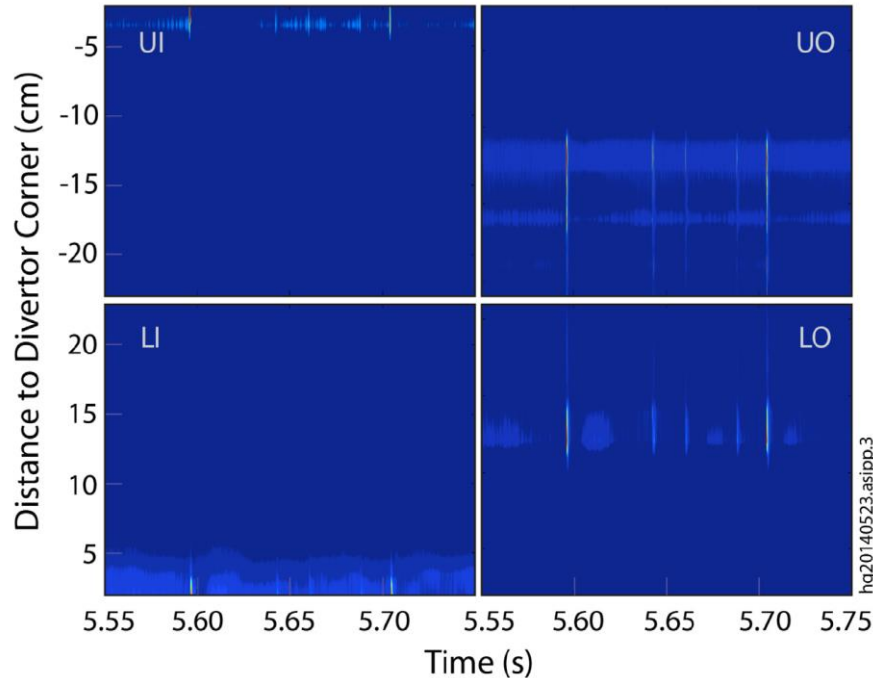


## EAST measurements\*

$q_t$  (MW/cm<sup>2</sup>)

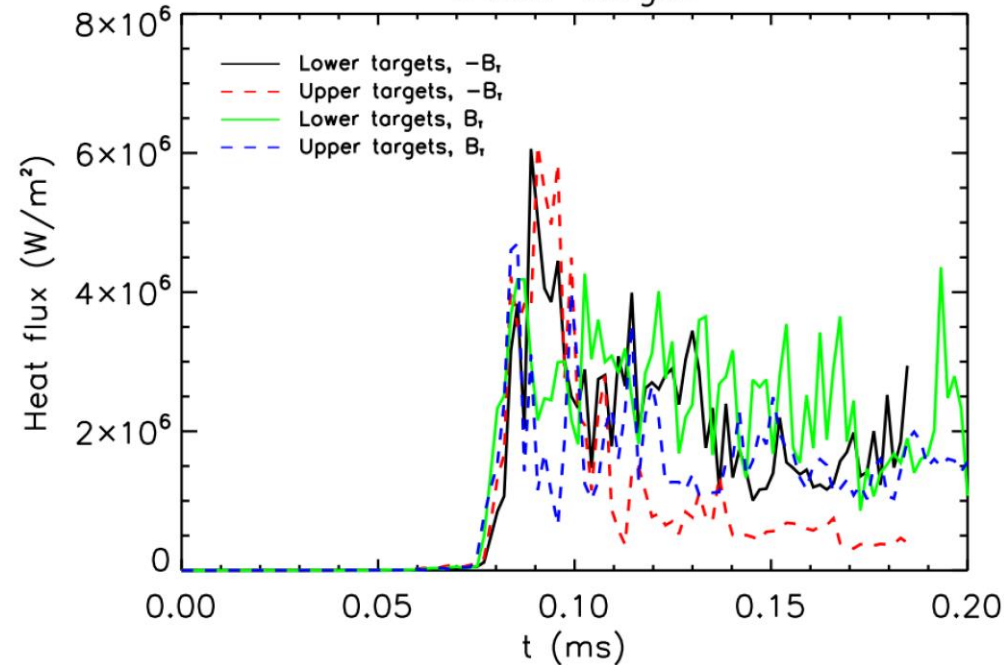


(Shot 42023)



## BOUT++ simulation

Outer target



Both experiments and BOUT++ simulations show the symmetric distribution of heat fluxes on upper and lower targets.



- Introductions
- Applications for divertor simulations
  - Transient heat flux simulations during ELM bursts on DIII-D
    - ◆ Kinetic modification on thermal conduction in pedestal
    - ◆ Validation with experiments
    - ◆ Study on the effects of magnetic flutter in parallel conduction
  - Transient particle flux simulations during ELM bursts on EAST
  - **Summary for divertor simulations**
- Demo for running 6-field



# Summary



- 6-field 2-fluid module in BOUT++ is developed to simulate the heat flux evolution during ELMs within real tokamak H-mode discharge parameters.
- In DIII-D H-mode discharge #144382, the parallel conduction is dominant by free streaming because of low collisionality.
  - Discussions of the effects of flux limiting coefficients  $\alpha_j$  : free streaming limit and sheath limit in H-mode simulations
    - ✓ The larger  $\alpha_j$  leads to the larger conductive flux, but smaller convective fluxes. because more energy are deposited to conductive flux by larger thermal conduction.
    - ✓ Compared to DIII-D diagnostics, the sheath limit of  $\alpha_j$  is the most reasonable coefficients to simulate the H-mode heat flux on divertor targets.
    - ✓ The magnetic flutter is effective to broaden the heat flux width on targets.
  - Within the sheath limit thermal conduction, our simulation shows the consistent energy loss, profile crash and heat fluxes with DIII-D diagnostics.
- The simulations gives the consistent asymmetric distribution of particle fluxes and symmetric heat fluxes on divertor targets to the EAST experiments.



- Introductions
- Applications for divertor simulations
  - Transient heat flux simulations during ELM bursts on DIII-D
    - ◆ Kinetic modification on thermal conduction in pedestal
    - ◆ Validation with experiments
    - ◆ Study on the effects of magnetic flutter in parallel conduction
  - Transient particle flux simulations during ELM bursts on EAST
  - Summary for divertor simulations
- Demo for running 6-field



# Simplified 6-field model in BOUT++



$$\frac{\partial}{\partial t} \varpi = -\frac{1}{B_0} \mathbf{b} \times \nabla_{\perp} \Phi \cdot \nabla \varpi + B_0^2 \nabla_{\parallel} \left( \frac{J_{\parallel}}{B_0} \right) + 2 \mathbf{b} \times \boldsymbol{\kappa} \cdot \nabla p_i + \mu_{\parallel i} \nabla_{\parallel 0}^2 \varpi,$$

$$\frac{\partial}{\partial t} n_i = -\frac{1}{B_0} \mathbf{b} \times \nabla_{\perp} \Phi \cdot \nabla n_i - n_i B_0 \nabla_{\parallel} \left( \frac{V_{\parallel i}}{B_0} \right),$$

$$\frac{\partial}{\partial t} V_{\parallel i} = -\frac{1}{B_0} \mathbf{b} \times \nabla_{\perp} \Phi \cdot \nabla V_{\parallel i} - \frac{1}{m_i n_{i0}} \mathbf{b} \cdot \nabla P,$$

$$\frac{\partial}{\partial t} A_{\parallel} = -\nabla_{\parallel} \phi + \frac{\eta}{\mu_0} \nabla_{\perp}^2 A_{\parallel} - \frac{\eta_H}{\mu_0} \nabla_{\perp}^4 A_{\parallel}$$

$$\frac{\partial}{\partial t} T_i = -\frac{1}{B_0} \mathbf{b} \times \nabla_{\perp} \Phi \cdot \nabla T_i - \frac{2}{3} T_i B_0 \nabla_{\parallel} \left( \frac{V_{\parallel i}}{B_0} \right) + \frac{2}{3 n_{i0} k_B} \nabla_{\parallel 0} (\kappa_{\parallel i} \nabla_{\parallel 0} T_i),$$

$$\frac{\partial}{\partial t} T_e = -\frac{1}{B_0} \mathbf{b} \times \nabla_{\perp} \Phi \cdot \nabla T_e - \frac{2}{3} T_e B_0 \nabla_{\parallel} \left( \frac{V_{\parallel e}}{B_0} \right) + \frac{2}{3 n_{e0} k_B} \nabla_{\parallel 0} (\kappa_{\parallel e} \nabla_{\parallel 0} T_e).$$

- Parallel velocity terms
- Parallel viscosity
- Hyper resistivity
- Thermal conduction

Switch Name	Physics meanings
compress0	Parallel velocity
viscos_par	Parallel viscosity
spitzer_resist	Spitzer resistivity
hyperresist	Hyper resistivity
diffusion_par	Thermal conduction



# 6-field model in BOUT++ (cont.)



Definitions:

$$\varpi = n_{i0} \frac{m_i}{B_0} \left( \nabla_{\perp}^2 \phi + \frac{1}{n_{i0}} \nabla_{\perp} \phi \cdot \nabla_{\perp} n_{i0} + \frac{1}{n_{i0} Z_i e} \nabla_{\perp}^2 p_{i1} \right),$$

$$J_{\parallel} = J_{\parallel 0} - \frac{1}{\mu_0} B_0 \nabla_{\perp}^2 \psi,$$

$$V_{\parallel e} = V_{\parallel i} + \frac{1}{\mu_0 Z_i e n_i} \nabla_{\perp}^2 A_{\parallel}.$$

$$\eta_{SP} = 0.51 \times 1.03 \times 10^{-4} Z_i \ln \Lambda T^{-3/2} \Omega \text{ m}^{-1}$$

Flux limited expression for parallel thermal conduction:

$$\kappa_{\parallel i} = 3.9 n_i v_{\text{th},i}^2 / \nu_i \quad \kappa_{\parallel e} = 3.2 n_e v_{\text{th},e}^2 / \nu_e$$

$$\kappa_{\text{fs},j} = n_j v_{\text{th},j} q R_0$$

$$\kappa_{\text{eff},j} = \frac{\kappa_{\parallel j} \kappa_{\text{fs},j}}{\kappa_{\parallel j} + \kappa_{\text{fs},j}}.$$



# Boundary conditions and normalizations



Boundary conditions:

Inner boundary:

$$\partial n_i / \partial \Psi = 0, \partial T_j / \partial \Psi = 0, \varpi = 0, \nabla_{\perp}^2 A_{\parallel} = 0, \partial^2 \phi / \partial^2 \Psi = 0, \partial V_{\parallel} / \partial \Psi = 0$$

Outer boundary:

$$n_i = 0, T_j = 0, \varpi = 0, \nabla_{\perp}^2 A_{\parallel} = 0, \partial^2 \phi / \partial^2 \Psi = 0, V_{\parallel} = 0$$

Normalizations:

$$\begin{aligned} \hat{T}_j &= \frac{T_j}{\bar{T}_j}, & \hat{n} &= \frac{n_i}{\bar{n}}, & \hat{L} &= \frac{L}{\bar{L}}, \\ \hat{t} &= \frac{t}{\bar{t}}, & \hat{B} &= \frac{B}{\bar{B}}, & \hat{J} &= \frac{\mu_0 \bar{L}}{B_0} J, \\ \hat{\psi} &= \frac{\psi}{\bar{L}}, & \hat{\phi} &= \frac{\bar{t}}{L^2 B_0} \phi, & \hat{\varpi} &= \frac{\bar{t}}{m_i \bar{n}} \varpi, \\ \tau &= \frac{\bar{T}_i}{\bar{T}_e}, & \hat{V} &= \frac{V}{V_A}, & V_A &= \frac{\bar{L}}{\bar{t}} = \frac{\bar{B}}{\sqrt{\mu_0 m_i \bar{n}_i}}, \\ \hat{P}_j &= \frac{P_j}{k_B \bar{n} \bar{T}_j}, & \hat{\kappa} &= \bar{L} \kappa, & \hat{\nabla} &= \bar{L} \nabla \end{aligned}$$



# Density profile as the input



Density profile used in 6-field model:

$$n_{i0}(x) = \frac{(n_{\text{height}} \times n_{\text{ped}})}{2} \left[ 1 - \tanh \left( \frac{x - x_{\text{ped}}}{\Delta x_{\text{ped}}} \right) \right] + n_{\text{ave}} \times n_{\text{ped}},$$

The coefficients in BOUT.inp:

```
[highbeta]
#hyperbolic tanh profile, N0 = N0tanh(n0_height*Nbar, n0_ave*Nbar, n0_width, n0_center)
n0_fake_prof = true      #use the hyperbolic profile of n0. If both n0_fake_prof and T0_fake_prof
n0_height = 0.           #the total height of profile of N0, in percentage of Ni_x
n0_ave = 0.2             #the constant tail of N0 profile, in percentage of Ni_x
n0_width = 0.1          #the width of the gradient of N0, in percentage of x
n0_center = 0.633       #the the center of N0, in percentage of x
n0_bottom_x = 0.81      #the start of flat region of N0 on SOL side, in percentage of x
```



# Compiling and running of 6-field module



For the exercise, a simple linear test is prepared:

Compiling:

Set the environment first, then

> make

Go to the scratch directory to run the code:

> cd \$SCRATCH

> cp -r \$BOUT\_TOP/examples/6field-simple/ .

> cp \$BOUT\_TOP/examples/6field-simple/  
cbm18\_dens8.grid\_nx68ny64.nc .

> cd 6field-simple/

Edit the pbs file with:

**#PBS -l advres=bout.10**

Submit job and run the job:

> qsub bout\_hopper\_debug.cmd

Data post-processing:

Add the idl library directory first

IDL> **!path=!path+":\$BOUT\_TOP/tools/idllib"**

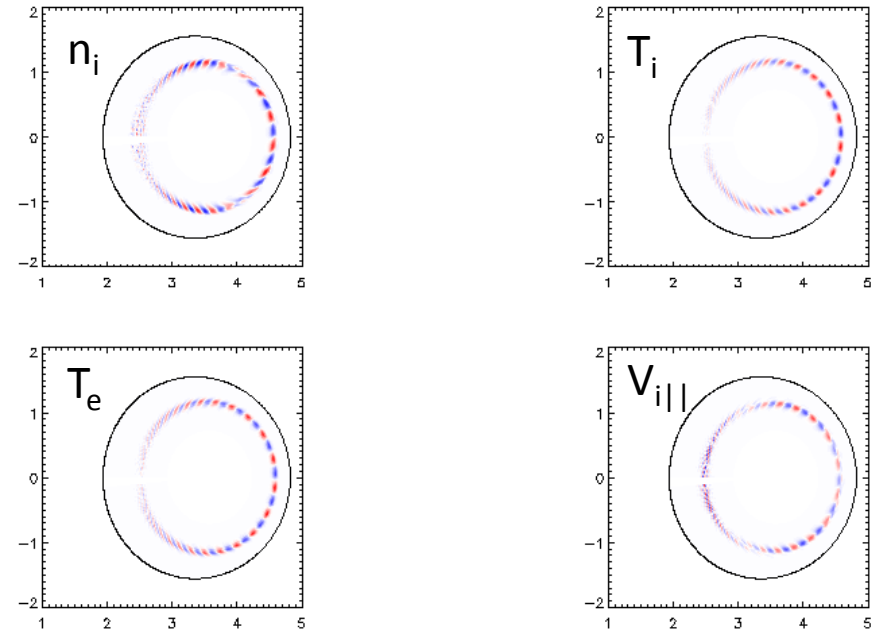
IDL> @collect-all

DCJP	FLOAT	= Array[68, 64, 101]
DCNI	FLOAT	= Array[68, 64, 101]
DCP	FLOAT	= Array[68, 64, 101]
DCPH	FLOAT	= Array[68, 64, 101]
DCPS	FLOAT	= Array[68, 64, 101]
DCTE	FLOAT	= Array[68, 64, 101]
DCTI	FLOAT	= Array[68, 64, 101]
DCU	FLOAT	= Array[68, 64, 101]
DCVP	FLOAT	= Array[68, 64, 101]
G	STRUCT	= -> <Anonymous> Array[1]
GR	FLOAT	= Array[1, 1, 101]
JP	FLOAT	= Array[68, 64, 16, 101]
NI	FLOAT	= Array[68, 64, 16, 101]
P	FLOAT	= Array[68, 64, 16, 101]
PH	FLOAT	= Array[68, 64, 16, 101]
PS	FLOAT	= Array[68, 64, 16, 101]
PSN	DOUBLE	= Array[68]
RMSJP	FLOAT	= Array[68, 64, 101]
RMSNI	FLOAT	= Array[68, 64, 101]
RMSP	FLOAT	= Array[68, 64, 101]
RMSPH	FLOAT	= Array[68, 64, 101]
RMSPS	FLOAT	= Array[68, 64, 101]
RMSTE	FLOAT	= Array[68, 64, 101]
RMSTI	FLOAT	= Array[68, 64, 101]
RMSU	FLOAT	= Array[68, 64, 101]
RMSVP	FLOAT	= Array[68, 64, 101]
TE	FLOAT	= Array[68, 64, 16, 101]
TI	FLOAT	= Array[68, 64, 16, 101]
U	FLOAT	= Array[68, 64, 16, 101]
VP	FLOAT	= Array[68, 64, 16, 101]

Variables after the collecting



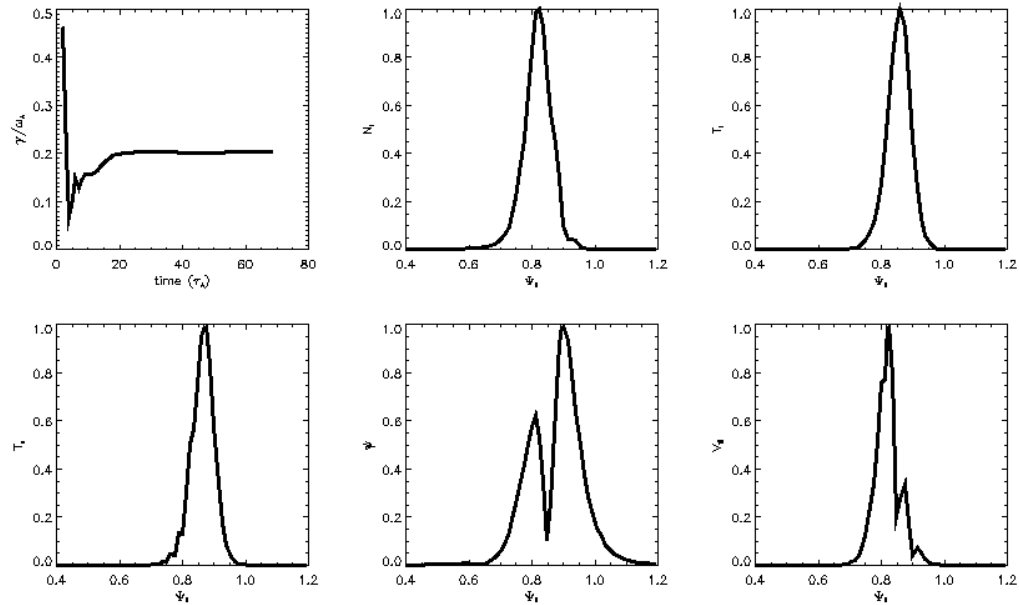
# The output of the mode structure (1)



Poloidal mode structures

$n0\_height = 0.0$   
 $n0\_ave = 0.2$

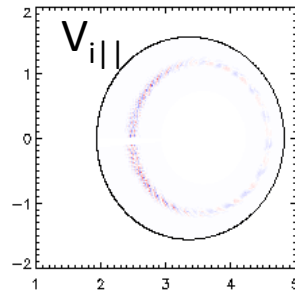
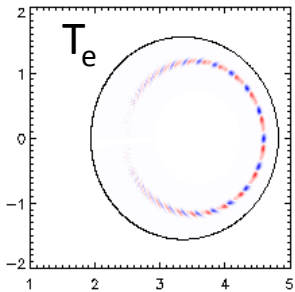
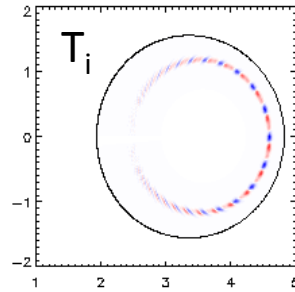
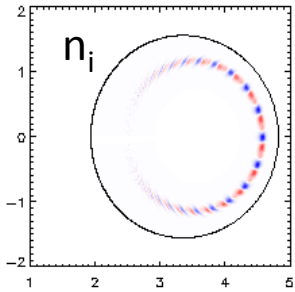
Linear growth rate for this test case:  
`IDL> print,gr[-1]`  
 0.202673



Linear growth rate and radial mode structures



# The output of the mode structure (2)



Poloidal mode structures

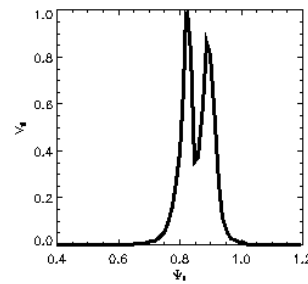
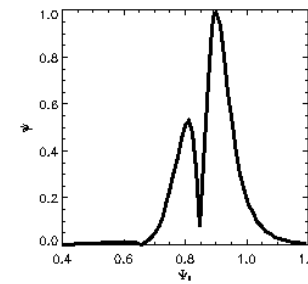
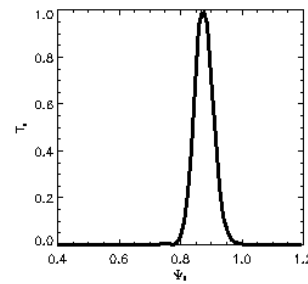
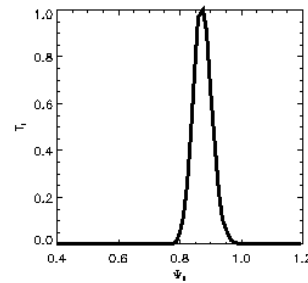
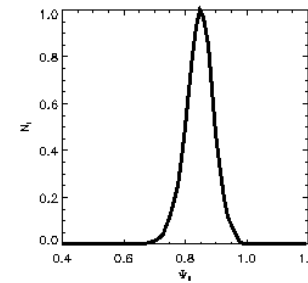
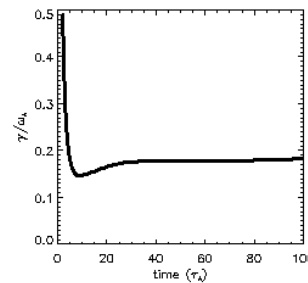
$n0\_height = 0.364$

$n0\_ave = 0.2$

Linear growth rate for this test case:

`IDL> print,gr[-1]`

0.183418

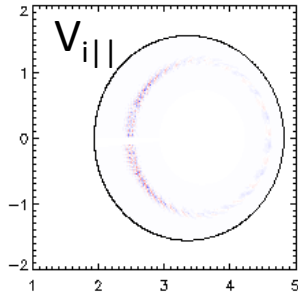
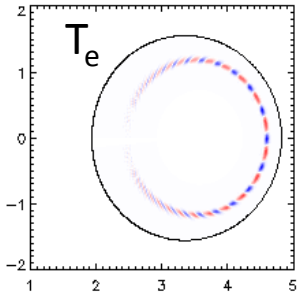
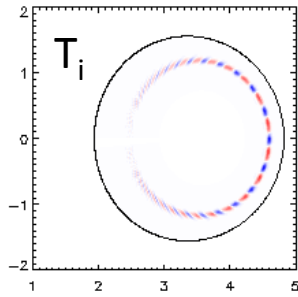
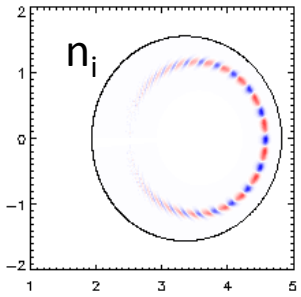


Linear growth rate and radial mode structures

mode structures



# The output of the mode structure (3)



Poloidal mode structures

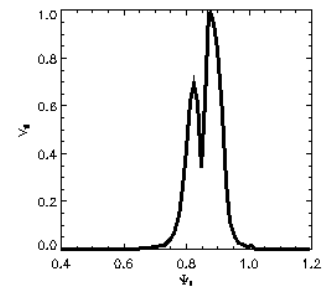
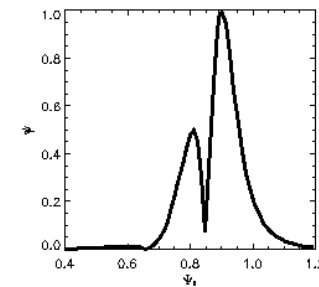
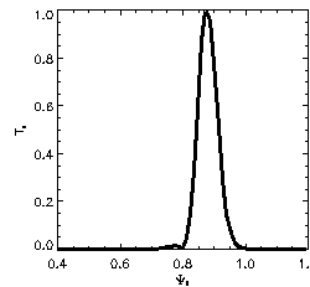
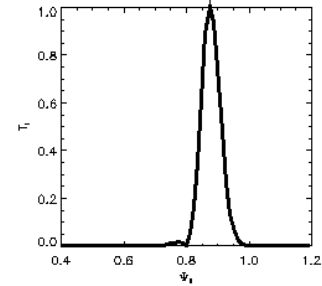
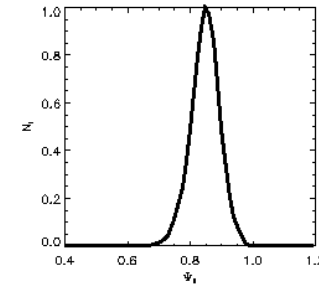
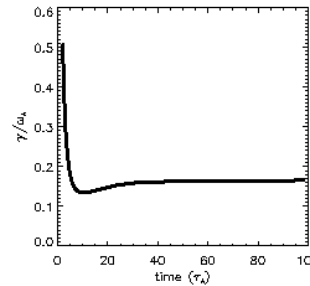
$n0\_height = 0.6$

$n0\_ave = 0.2$

Linear growth rate for this test case:

`IDL> print,gr[-1]`

0.166440



Linear growth rate and radial mode structures

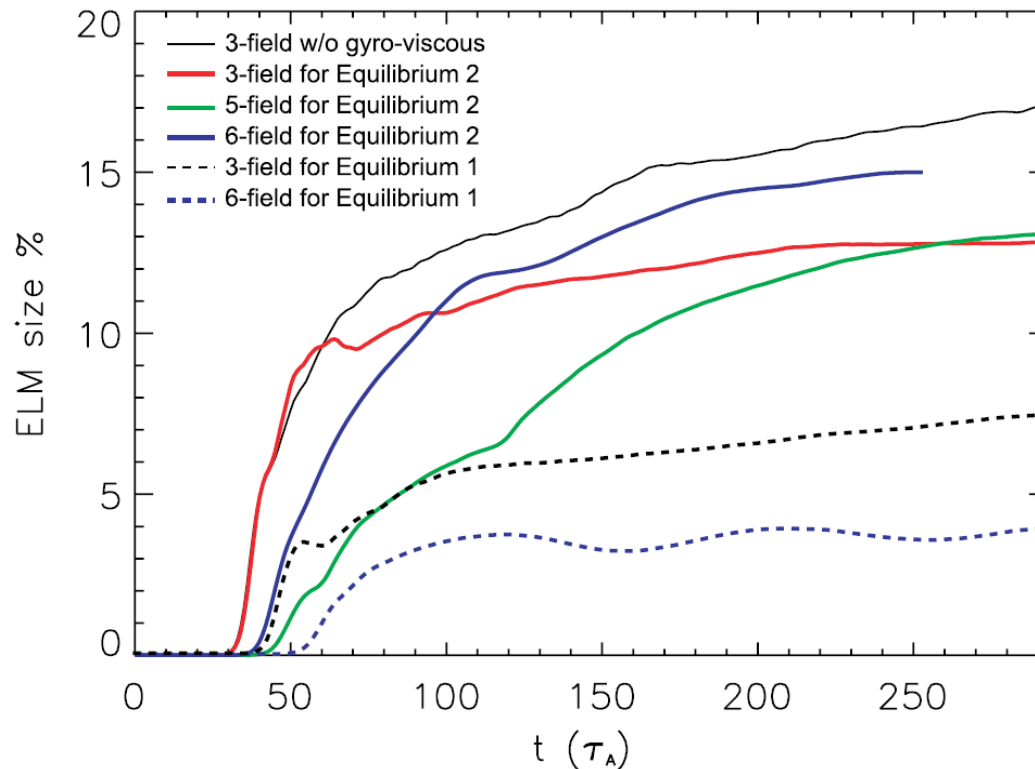


# Backup slides





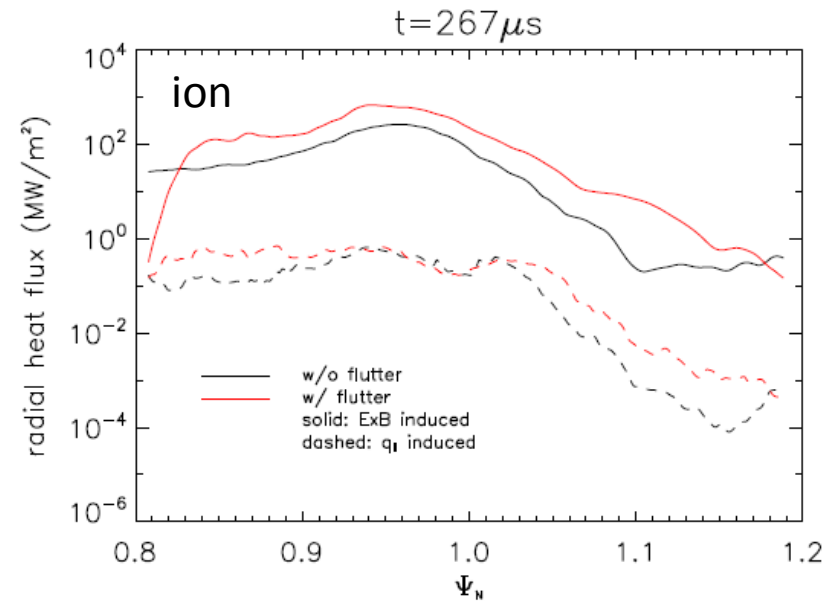
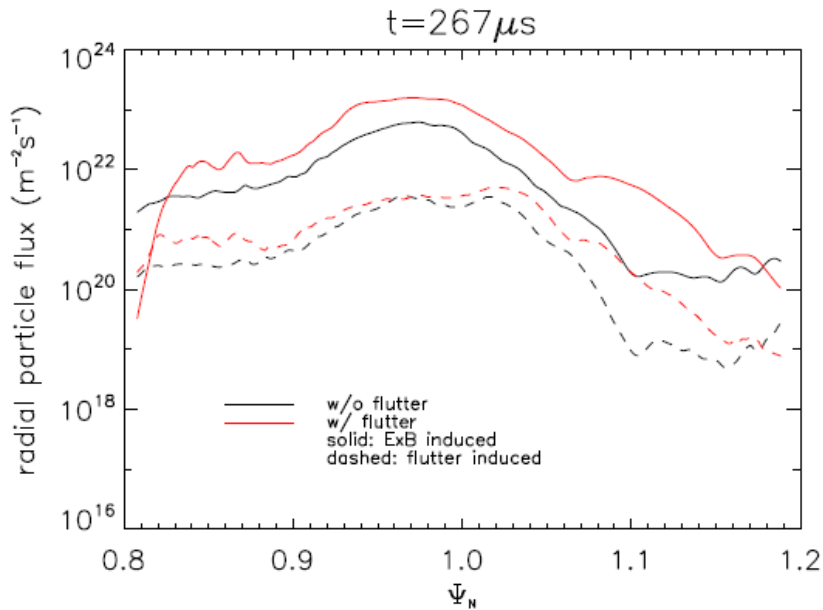
# Nonlinear comparison with 3-field model



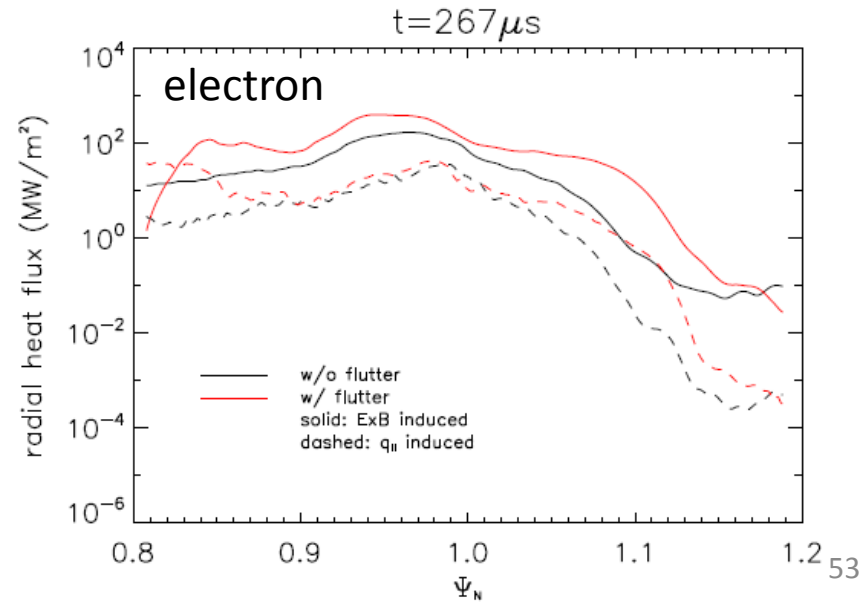
- For weaker P-B unstable equilibrium (1), both three-field and six-field models show the consistent results at linear and nonlinear phases.
- In stronger P-B unstable equilibrium (2), while additional terms of six-field do enhance the instability.
- The six-field model yields smaller ELM size than 3-field model in both equilibria.



# The magnetic flutter enhance radial transport



- Radial particle flux and heat fluxes are all enhanced by magnetic flutter
- More effective on ion heat flux than electron.
- The effects of magnetic flutter are mainly on the ExB induced fluxes
- The non-consistent calculation of conductive fluxes are similar to the consistent one, especially near the separatrix.





# Simulations show the filaments of ELMs and heat load strips on targets

